Applied Catalysis B: Environmental 218 (2017) 119–136

Contents lists available at ScienceDirect

Applied Catalysis B: Environmental

journal homepage: www.elsevier.com/locate/apcatb

Reactivity of novel Ceria–Perovskite composites CeO_2- $LaMO_3$ (MCu, Fe) in the catalytic wet peroxidative oxidation of the new emergent pollutant 'Bisphenol F': Characterization, kinetic and mechanism studies

Samia Ben Hammouda [a,*], Feiping Zhao [a], Zahra Safaei [a], Indu Babu [a], Deepika Lakshmi Ramasamy [a], Mika Sillanpää [a,b,**]

[a] Laboratory of Green Chemistry, School of Engineering Science, Lappeenranta University of Technology, Sammonkatu 12, FI-50130 Mikkeli, Finland
[b] Department of Civil and Environmental Engineering, Florida International University, Miami, FL 33174, USA

ARTICLE INFO

Article history:
Received 17 April 2017
Received in revised form 2 June 2017
Accepted 17 June 2017
Available online 20 June 2017

Keywords:
Perovskite
Ceria
Fenton
Heterogeneous
Bisphenol F

ABSTRACT

In the present study, ceria, pristine perovskites $LaMO_3$ (Cu, Fe) and novel ceria-perovskite composites CeO_2-$LaMO_3$ were successfully prepared and applied as heterogeneous Fenton like- catalysts for the degradation and mineralization of a new emergent compound- bisphenol F (BPF) in aqueous solution. The catalysts were characterized by X-ray diffraction spectrometer (XRD), BET surface area determination, scanning electron microscopy (SEM), Energy Dispersive X-ray (EDS) and X-ray photoelectron spectroscopy (XPS) techniques. Catalytic bisphenol F behavior shows that the activity of pristine perovskites was improved due to the introduction of cerium. Catalytic activity in terms of TOC removal followed the order of CeO_2-$LaCuO_3$ > CeO_2-$LaFeO_3$ > $LaCuO_3$ > $LaFeO_3$ > CeO_2 with about 83, 79, 68, 64 and 28% respectively. Only the novel composite oxide CeO_2-$LaCuO_3$ was found to be effective for Bisphenol F degradation at neutral conditions. EPR analyses and scavenging experiments revealed that BPF was mainly decomposed by the attack of $^{\bullet}OH$, especially the surface-bounded $^{\bullet}OH$. BPF decay followed pseudo-first-order reaction kinetics. The absolute rate constant for BPF oxidation by $^{\bullet}OH$ was found to 2.0910^9 M^{-1} s^{-1}, as determined by the competition kinetic method. Six stable organics intermediates were observed and five of them were identified *p*-benzoquinone, hydroquinone, 4-hydroxybenzaldehyde and Bis (4-hyroxyphenyl) methanol. Subsequent attack of these intermediates by $^{\bullet}OH$ radicals led to the formation of short chain acids: malonic, succinic, acetic, formic and oxalic acids. On the basis of the analytical results for the intermediate products and the assumption that hydroxyls radicals are the major reactive species, a plausible pathway of BPF mineralization during the heterogeneous Fenton process was proposed. Furthermore, the CeO_2-$LaCuO_3$ composite exhibited excellent long-term stability in the heterogeneous Fenton-like process. These results suggested that the novel ceria perovskite material would be a promising candidate for practical wastewater treatment.

© 2017 Elsevier B.V. All rights reserved.

1. Introduction

Bisphenol compounds are a class of organic chemicals commonly used in the production of polycarbonate plastics and epoxy resins which are extensively employed in the manufacturing of varnishes, plastic containers, food and drink packaging, bottles, medical materials, lens, toys and many others products [1]. Bisphenol A (4,4′-dihydroxydiphenyl-propane, BPA) is the most widely used bisphenol, with more than 8 billion pounds produced each year [2]. Faced with increasing concern due to its potential adverse human health impacts, BPA has been banned in certain products in many countries, such as Canada, France and in the European Union [3]. To comply with regulations, bisphenol analogs, including bisphenol F(4,4′-dihydroxydiphenylmethane, BPF) have been introduced into the global markets [4–7]. As well as its structural analog bisphenol A, BPF has endocrine disrupting effects and

* Corresponding author at.
** Corresponding author at: Laboratory of Green Chemistry, School of Engineering Science, Lappeenranta University of Technology, Sammonkatu 12, FI-50130 Mikkeli, Finland.
E-mail addresses: Samiabenhammouda@gmail.com, Samia.Ben.Hammouda@lut.fi (S.B. Hammouda), mika.sillanpaa@lut.fi (M. Sillanpää).

http://dx.doi.org/10.1016/j.apcatb.2017.06.047
0926-3373/© 2017 Elsevier B.V. All rights reserved.

also was found to have genotoxic potential and other toxicological profile similar to BPA [8–14]. The detection of Bisphenols F in environmental media has significantly increased in the last decade due to their widespread use. Thus, their fates in aquatic and terrestrial environmental merits close attention in terms of both human and environmental risks.

To date, only a few studies are available on the treatment of bisphenol F and most of them are dedicated to the bioremediation. Inoue et al. [15] reported the biodegradation of BPF by a bacterium isolated from river water, Sphingobium yanoikuyae. In other study Ike et al. [16] investigated the BPF biodegradation by river water microorganisms under aerobic and anaerobic conditions. The degradation of BPF by a bacterial consortium enriched with ammonium nitrate has been studied recently by Lu et al. [17]. Sea water microorganisms were used by Danzel et al. [8] and a complete degradation of BPF was obtained within 30 days. Biological treatment requires several days or weeks [18,19] and therefore cannot be used in sites where immediate action is required. Thus, rapid and efficient treatment processes must be developed for the bisphenol remediation.

Advanced oxidation processes, which involve the generation of highly potent chemical species, are considered the most effective technologies for water and wastewater treatment [20–22]. The Fenton process has so far been the preferred process used in the treatment of refractory organic compounds in aqueous wastes due to its relative low cost, easy operation and its strong oxidative capacity. The conventional homogeneous Fenton process is limited by the narrow working pH range (<4) and the formation of ferric hydroxide sludge that requires further separation and proper disposal. To overcome these drawbacks, the development of heterogeneous Fenton catalysts has gained intensive attention over the last decade. Several Fenton-like catalysts using clays [23], polysaccharide [24,25], activated carbon [26,27], zeolites [28,29], silicas [30], nafion [31], resins [32,33], hydrotalcites, and various other materials as solid support for the Fenton reaction have been reported [34,35].

Perovskite-type oxides, described by the general formula ABO (ABO_3), have attracted extensive attention of researchers and have been reported as promising catalysts in oxidation, hydrogenation and hydrogenolysis reactions owing their unique structural features, high redox properties and the great flexibility of their crystal lattice to accommodate cation substitutions. Although perovskites have been largely studied in various fields, especially for electronic and energy utilization, perovskites investigation as heterogeneous catalysts for water treatment is still rather limited [37–42].

In spite of their good performances, the main limitation of using perovskites on a large scale emerges from their reduced ability to develop large surface areas [43]. Up to now, zirconia, aluminum and silicon oxides have been used in order to increase the contact surface between the perovskite and the reactant species by deposition on adequate supports [44–46].

Among various support surfaces, Ceria has gained great attention due to the Ce^{3+}/Ce^{4+} redox process and high oxygen storage capacity, which improve the catalytic ability of a material for use in wastewater treatment. Ceria based catalysts were investigated for catalytic wet air oxidation and catalytic wet peroxide oxidation techniques. It has also been reported that ceria has a significant positive effect on the catalytic, oxygen storage redox and thermal properties of catalysts. Interestingly, Alifanti et al. reported that ceria containing materials are promising as supports due to their inability to enter into the perovskite lattice with any of the most used cations for environmental purposes, e.g. La, Co, Mn or Fe [43,47]. The ceria support should represent a good choice due to its high surface area and moderate interactions with perovskite. Some supported perovskite ceria phases have already been reported in the literature for various applications. Shin et al. [48] reported CeO_2-$LaFeO_3$ composite oxide as an active anode for direct hydrocarbon-type solid oxide fuel cells. Doped CeO_2-$LaFeO_3$ composite has also been reported by Liu et al. [49] as both anode and cathode for solid oxide fuel cells. In another study, the effect of Ce on the structural features and catalytic properties of $LaCeFeO_3$ perovskite-like has been investigated by Sun et al. [36] for the production of hydrogen from simulated coal-derived syngas via the high temperature water-gas shift reaction. Ceria-based oxides as supports for $LaCoO_3$ perovskite has also been reported for the total volatile organic compounds (VOC) oxidation by Alifanti et al. [43]. The authors showed that the deposition of $LaCoO_3$ on ceria-based supports brings an improvement in the specific activity with respect to bulk perovskite.

Similarly to the classical Fenton reaction which involves iron as catalyst, the decomposition of hydrogen peroxide to hydroxyl radicals could be catalyzed by other transition metal ions such as cobalt, silver and copper.

Recently, Cu-based catalysts have attracted a great deal of attention because the redox properties of copper are similar to iron, and the Cu-based Fenton-like process could work over a broader pH range compared to the Fe-based redox system.

Various materials were developed as catalyst supports for use in the catalytic wet peroxide oxidation; these were zeolites, mixed oxides and hydroxides, pillared clays etc. Nevertheless, even though some of the catalysts were highly active, their stability often was unsatisfactory due to leaching of the active component in the aggressive aqueous oxidative medium. Apart from its high activity, the inorganic perovskite structure has shown higher stability than any other material. The catalytic versatility of perovskite oxides is attributed to their great stability at high temperature and in an aggressive medium, as well as to the high oxygen mobility and the stabilization of transition metal ions in unusual high oxidation states.

In this paper, ceria-doped $LaCuO_3$ and $LaFeO_3$ perovskite were prepared, characterized, and assessed for Fenton catalysis in the presence of hydrogen peroxide. To the best of our knowledge, Ceria-perovskite oxides have never been investigated previously for hydrogen peroxide activation. Also, no previous studies have investigated the use of ceria-lanthanum based copper perovskite as catalysts for wastewater treatment.

Ceria, pristine perovskites $LaMO_3$ (Cu, Fe) and ceria-perovskite composites CeO_2-$LaMO_3$ were synthesized by the calcination, citric acid sol-gel and impregnation method, respectively. The as prepared catalysts were characterized by means of nitrogen isotherm adsorption, scanning electron microscopy (SEM), X-ray diffraction (XRD) and x-ray photoelectron spectroscopy (XPS). To probe in the mechanism of H_2O_2 activated by perovskite catalysts, quenching radical tests and Electron paramagnetic resonance (EPR) spectroscopic analysis was performed. The effectiveness of $LaMO_3$ and H_2O_2 combination has been investigated varying concentration, catalyst dosage and solution pH, which are the main operating variables. Catalyst reusability has also been assessed. Based on the identified cyclic intermediates and carboxylic acids as end products before mineralization, a plausible mineralization pathway was proposed. Finally, a special attention was devoted to the reusability of the composite catalyst.

2. Experimental

2.1. Chemicals

Bisphenol F(4,4′-dihydroxydiphenyl-methane, BPF), $La(NO_3)_3{\cdot}6H_20$, $Ce(NO_3)_36H_2O$, $Fe(NO_3)_3{\cdot}9H_20$ and $Cu(NO_3)_3{\cdot}4H_20$, citric acid, hydrogen peroxide, 5,5-Dimethyl-1-pyrroline-N-oxide (DMPO) were provided by Sigma-Aldrich.

All reagents were of analytical grade and were used as received without further purification. Deionized water was employed throughout this study. For the pH adjustment, diluted solution of sulfuric acid or sodium hydroxide was employed.

2.2. Catalysts preparation

Based on the literature [50], the CeO_2 nano-sized porous support was synthesized by the calcination method: the precursor cerium nitrate $Ce(NO_3)_3{\cdot}6H_2O$ was directly calcined at 500 °C in air atmosphere for 4 h. Ceria can be synthesized by various methods but the calcination of nitrates was reported as the simplest, cheapest and the most environmental-friendly one, since solvents, surfactants, templates or chemical reactants are not required [50].

The composite catalysts Ceria- perovskite CeO_2-$LaMO_3$ (M = Cu, Fe) (Fig. S_1) were prepared by the impregnation method. Briefly, CeO_2 (2 g) was impregnated with a 500 mL mixed aqueous solution of metal nitrates(i.e., 0.1 M) and citric acid with a molar ratio of La:M:citric acid = 1:1:2. After stirring continuously for 2 h, the resultant solution was heated 12 h over 100 °C to evaporate water. The obtained sol-like solution was subsequently dried at 100 °C for 24 h, grinded and then calcinated at 700 °C for 5 h in air. All the materials were stored in a desiccator under ambient temperature for further experiments. For the highest catalytic activity, the catalyst CeO_2-$LaCuO_3$ was used for all of the experiments unless otherwise specified.

$LaMO_3$ (without CeO_2 support) was also prepared for comparison using the aforementioned procedure in the absence of CeO_2.

2.3. Characterization

The powder (XRD) patterns of the catalysts were recorded on a PANalytical Empyrean diffractometerwith Co-Kα (λ = 1.7809 Å) radiation source. The generator voltage and tube current used were 40 kV and 40 mA, respectively. The diffraction angle (2θ) ranged from 20° and 80° in 0.05° intervals. The crystalline size was estimated by the Scherer equation Eq. (1).

$$\mathbf{D}(\mathbf{h}kl) = \frac{\mathbf{K}\lambda}{\beta \mathbf{Cos}\theta} \quad (1)$$

Where D is the crystallite size perpendicular to the normal line of the (*hkl*) plane, K is the Debye-Scherrer constant (0.89), *hkl* the full width at half maximum (fwhm) of the (*hkl*) diffraction peak, *hkl* the Bragg angle of the (*hkl*) peak, and λ the X-ray wavelength.

Microstructure and morphology of the synthesized materials were carried out using (SEM). The elemental composition of the pure perovskite and ceria-perovskite composites was determined using (EDS). The EDS analysis was performed at several points and averaged to obtain the representative results.

Nitrogen adsorption/desorption experiment were used for textural studies with Micromeritics' TriStar II PLUS instrument. All the studied samples were pre-degassed in vacuum at 200 °C for 2 h. Specific surface area were determined using the classical BET model. The study of the surface composition and the electronic states of elements in the valence-band region of the perovskite oxides were recorded on a ESCALAB 250 X-ray photoelectron spectroscopy (XPS) with Al-Kα (1486,6 eV) as the X-ray source.

Reactive oxygen species (ROS) were detected by electron spin resonance spectroscopy using DMPO as a spin trap agent. The EPR spectra were obtained using a CMS-8400 paramagnetic resonance spectrometer. The operating conditions were as following: magnetic field 336.5 ± 6.0 mT width, power attenuation 10 dB, field modulation 0.100 mT, sweep time 100 s, microwave frequency 9450 MHz.

2.4. Experimental procedure

The treatment of bisphenol F by heterogeneous Fenton system was conducted by batch-type experiments. Prior to the addition of hydrogen peroxide, the required amount of catalyst was added to 100 mL of BPF solution with an initial concentration of 20 mg L^{-1} and magnetically stirred for about 30 min to establish the adsorption equilibrium between the BPF molecules and the catalyst. A known concentration of H_2O_2 was added to the solution to initiate the reaction. At given time intervals, samples of 1 mL were withdrawn from the reactor and filtered immediately through a 0.22 μm filter film for analysis.

For the catalyst reusability tests, after each run the catalyst was filtrated, washed thoroughly with deionized water, and then dried at 100 °C for 1 h for reuse under similar experimental conditions. The concentrations of La, Cu, Ce and Fe in the solutions after reaction were measured by inductively coupled plasma (ICP) using Thermo Scientific ICAP 6000 ICP.

2.5. Analytical methods

Bisphenol F concentration was quantified by a Shimadzu High Performance Liquid Chromatograpy equipped with UV detection (HPLC-UV). The column used was a Kinetex C18 (5 μm, 4.6 × 150 mm). A mobile phase composed by 20 mM (phosphoric-acid) potassium buffer solution (pH 2.5) (A)and acetonitrile (B) was pumped at a flow rate of 0.7 mL min^{-1}, with an isocratic percentage composition of 50:50 A:B. The UV detector wavelength was set at 229 nm with a column temperature of 30 °C. Observed retention time was around 6.79 min.

Generated carboxylic acids: Malonic, succinic, oxalic, formic and acetic acids, were identified and quantitatively followed by ion chromatography with suppressor equipped with a conductivity detector using a Shodex IC SI-50 4E (4.0mmI.D. × 250 mm). The eluent was 3.2 mM Na_2CO_3 and 1 mM $NaHCO_3$at a flow rate of 0.7 mL min^{-1}.

The bisphenol F intermediates were analyzed bygas chromatography – mass spectrometry(GC–MS) (Agilent-GC 6890N, MS 5975) with agilent DB-5MS GC column dimensions 30 m, 0.25 mm, 0.25 μm. The inlet temperature was 250 °C in split less mode and the injection volume was 1.0 μL. The oven temperature was programmed at 50 °C for 3 min and it raises at the rate of 5 °C/min to 300 °C held for 2 min.

Bisphenol F mineralization during the treatment was monitored by measuring the non-purgeable organic carbon (NPOC) abatement. The NPOC in samples was quantified by a TOC analyzer purchased from Shimadzu. Organic carbon compounds were combusted and converted to CO_2, which was detected and measured by a non-dispersive infrared detector (NDIR). Standard potassium hydrogen phthalate solutions were used as standards for the NPOC analysis.

3. Results and discussion

Catalysts characterization

The as-synthesized samples were first characterized by XRD diffraction measurements. The XRD patterns of CeO_2, $LaFeO_3$, $LaCuO_3$, CeO_2-$LaFeO_3$ and CeO_2-$LaCuO_3$ samples are depicted in Fig. 1. All the characteristic peaks of the pure perovskites were well assigned to $LaFeO_3$ [51] and $LaCuO_3$ [52]. The reflection peaks of ceria simple are in agreement with the cubic phase CeO_2 [53]. The XRD patterns of CeO_2-$LaCuO_3$ and CeO_2 $LaFeO_3$ composites mainly revealed diffraction peaks of $LaCuO_3$ and $LaFeO_3$, respectively. The characteristic diffraction peaks of ceria were also observed in the

Table 1
Crystallographic parameters of ceria, pristine perovskites and ceria-perovskite composites samples.

Sample	Crystal system	a (Å)	b (Å)	C (Å)	α (°)	β (°)	γ (°)	Density (g/cm^3)
CeO_2	Cubic	5.407	5.407	5.407	90	90	90	6.43
$LaFeO_3$	Orthorhombic	5.577	7.880	5.575	90	90	120	6.58
$LaFeO_3/CeO_2$	Orthorhombic	5.572	7.869	5.567	90	90	90	6.61
$LaCuO_3$	Orthorhombic	5.362	13.169	5.400	90	90	90	7.07
$LarCuO_3/CeO_2$	Orthorhombic	5.355	5.401	13.153	90	96.28	90	7.07

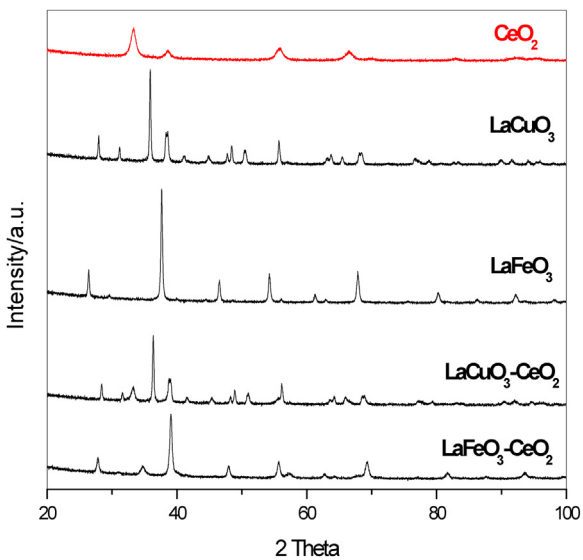

Fig. 1. XRD patterns of the as-prepared CeO_2, $LaFeO_3$, $LaCuO_3$, CeO_2-$LaFeO_3$ and CeO_2-$LaCuO_3$.

composites XRD patterns, which indicated that the composites might be formed by the ceria incorporation into the lattice of the perovskite structure. However, we cannot exclude the possibility that the composites were formed by the physical bond between perovskite and Ceria. The slight decrease in the intensity of the diffraction peaks observed in the XRD patterns of ceria-perovskites composites is mostly due to the dilution of perovskite structure by the ceria support. The diffraction peaks remain sharp but slightly shift in position, indicating a possible modification of the structural lattice parameters caused by the ceria incorporation. The crystallographic parameters of all the samples are illustrated in Table 1. Results showed that all the perovskite based catalysts had a single phase nature with the orthorhombic structure.

Based on the calculation with Scherrer equation (1), the average crystallite size of CeO_2, $LaCuO_3$, $LaFeO_3$, CeO_2-$LaCuO_3$ and CeO_2-$LaCuO_3$ was estimated to be about 39.2, 26.7, 28.6, 20.6 and 21.8 nm. Thus, the addition of ceria in perovskite lattice led to a smaller crystallite size. This observation is very important for the catalytic study, due to the fact that smaller particles possess higher surface area and provide more structural defects, which is beneficial for oxidative reaction [53,54].

The nitrogen adsorption/desorption measurements were also carried out to determine the specific surface areas and characteristics porosity of catalysts as summarized in Table 2. The composite catalysts show a considerable increase in the specific surface area. Likewise the ceria incorporation brings higher pore volume in the composite. This result is in good agreement with previous studies which report an increase in the specific surface area of materials after introduction of ceria. The BET surface area of the CeO_2-$LaFeO_3$ and CeO_2-$LaCuO_3$ was found to be 19.68 and 11.49m^2 g^{-1}, with corresponding volume of 0.0079 and 0.0048 cm^3 g^{-1}. The incorporation of ceria in the perovskite matrix results in increasing the specific area, thus providing a larger number of reactive edge

Table 2
Structural parameters of CeO_2, $LaFeO_3$, $LaCuO_3$, CeO_2-$LaFeO_3$ and CeO_2-$LaCuO_3$ samples.

Sample	BET surface area (m^2 g^{-1})	Pore volume (cm^3 g^{-1})	Pore size (nm)
CeO_2	65.6614	0.027531	10.882 Å
$LaFeO_3$	9.3580	0.003670	10.894
$LaCuO_3$	6.8753	0.002942	10.844
CeO_2-$LaFeO_3$	19.6775	0.007880	10.374
CeO_2-$LaCuO_3$	13.4867	0.004853	10.978

sites which would contribute to a better catalytic performance. The pore diameters of pristine and composite samples have no obvious change.

The morphological properties of the five catalysts was evaluated by (SEM). As shown in Fig. 2, ceria exhibited agglomeration of the particles with irregular shapes. This confirms the known character of ceria that aggregation unavoidably occurs during the combustion synthesis process. Interestingly, the SEM micrographs revealed that the $LaCuO_3$ structure exhibit a large number of pores with uniform size distribution. According to the literature [55], the observed tiny pores are mainly due to the gas evolution released during the bulk thermal decomposition of citric acid. Addition of ceria to the perovskite matrix changes the particle morphology and size. The CeO_2-Perovskite composite catalyst shows flake like texture and smaller particles, which agreed well with the XRD results. The textural properties are related to the swelling nature of the precursors. In the citrate system, the catalysts are prepared by rapid evacuation of the molten mixture of the corresponding salts and citric acid and subsequent calcination at 700 °C. Considerable swelling of the citrate precursor takes place in the presence of the metal salts contributing to the mutual dispersion of the oxide components.

In order to examine the elemental composition of the pristine samples and the ceria-perovskite composites, (EDX) mapping was recorded. Fig. 3 shows the EDS spectra acquired at top-view samples in SEM. They reveal the presence of La, Ce, O and Cu or Fe in concordance to the nominal chemical composition of the envisaged perovskite-ceria composite. Quantitative analysis of the EDS spectra shows that the weight percentage ratios of La/Cu/Ce and La/Fe/Ce are 44.6: 24.6: 8.7 and 48.3:15.2: 13.9 for CeO_2-$LaCuO_3$ composite and CeO_2-$LaFeO_3$, respectively. The small carbon signal which appears at around 0.2 Kev and the detected slight amount of aluminum are ascribed to the deposition of the samples on carbon tape on aluminum stub.

The surface chemical species and their oxidation states were examined by (XPS) and the results are presented in Figs. 4 and 5. A wide survey scan of XPS spectra was taken, the high-resolution spectrum of the La 3d region of $LaFeO_3$ and CeO_2-$LaFeO_3$ showed two peaks at binding energies (BE) of 834.9 and 851.3 eV which could be assigned to the La $3d_{5/2}$ and La $3d_{3/2}$ respectively, while two BE at 838.4 and 855.3 eV corresponded to their shake-up satellites [56]. Those BE peaks for $LaCuO_3$ and CeO_2-$LaCuO_3$ are situated at 833.4, 850.2, 837.7, and 854.6. Moreover, the BE difference (spin-orbit splitting) between peaks La $3d_{5/2}$ and La $3d_{3/2}$ equaled to 16.4 eV for $LaFeO_3$ and CeO_2-$LaFeO_3$ and 16.8 for $LaCuO_3$ and CeO_2-$LaCuO_3$, suggesting that predominant state of La(III) in the as-prepared catalysts [57].

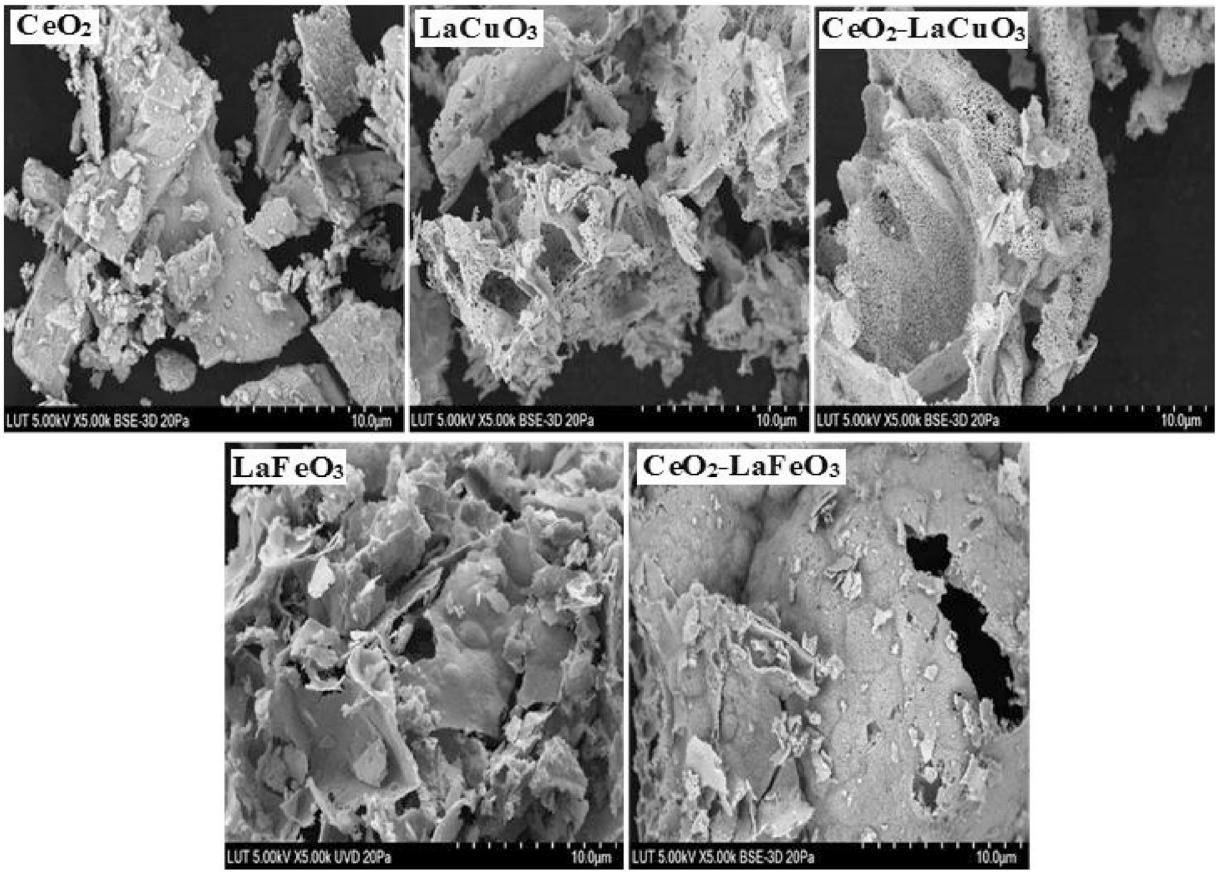

Fig. 2. SEM micrographs of synthesized CeO_2, $LaFeO_3$, $LaCuO_3$, CeO_2-$LaFeO_3$ and CeO_2-$LaCuO_3$.

Analysis of the Fe 2p spectra of $LaFeO_3$ and CeO_2-$LaFeO_3$ (Fig. 4) found the BE peaks at 710.7 and 724.3 eV, which are assigned to Fe $2p_{3/2}$ and Fe $2p_{1/2}$, respectively. There was not any noticeable shoulder peak observed in Fe 2p spectra of both $LaFeO_3$ and CeO_2-$LaFeO_3$, revealing that iron atoms are in the formal chemical valance state of +3 [58]. In the Cu 2p spectra of $LaCuO_3$ and CeO_2-$LaCuO_3$ (Fig. 5) the BE peak at 933.5 eV for Cu $2p_{3/2}$ and its shake-up contribution at about 943.4 eV revealed that the major state of Cu in the catalysts are Cu(II) [56]. O. Taran et al. have described that Cu(II) is the characteristic of Cu in perovskite unlike Fe and regardless of the stoichiometry (ABO_3) [59].

The Ce 3d spectra of CeO_2, CeO_2-$LaFeO_3$ and CeO_2-$LaCuO_3$ showed several doublets of peaks referring to Ce $3d_{5/2}$ (lower BE) and Ce $3d_{3/2}$ (higher BE). The doublets at 882.5/900.6 eV, 889.0/907.7 eV, 898.3/916.6 eV are ascribed to the $3d^{10}4f^0$ initial electronic state of Ce(IV). Importantly, the doublet at about 885/904 eV assigned to the $3d^{10}4f^1$ initial electronic state corresponding to Ce(III) [60] were not observed in the catalysts, indicating that the state of Ce in CeO_2, CeO_2-$LaFeO_3$ and CeO_2-$LaCuO_3$ are mostly Ce(IV).

The O 1s BE peaks at 529.0–529.3 eV are assigned to the lattice oxygen (O_L) for $LaFeO_3$, $LaCuO_3$, CeO_2, CeO_2-$LaFeO_3$, and CeO_2-$LaFeO_3$, while the component at 530.9–531.5 eV corresponds to the chemisorbed oxygen (O_{ads}) [58], which is the most active oxygen and has been reported to play an important role in the oxidation reaction [60].

3.2. Catalytic properties and stability of pristine perovskites and ceria doped perovskites

The Fenton catalytic activity of CeO_2-$LaMO_3$ (M = Fe, Cu) composites was studied using the degradation of bisphenol F as a probe reaction, and the results were compared with those of pure $LaMO_3$ (M = Fe, Cu) and CeO_2.

At first, it is important to mention that, without catalyst and oxidant, no change in the bisphenol F concentration was observed, indicating that the BPF solution could not self-decompose. Moreover, as shown in Fig. 6, BPF was very stable and hardly degraded in the presence of hydrogen peroxide only, which can be explained by the weaker oxidation potential of peroxide hydrogen (H_2O_2) in comparison with hydroxyl radicals ($^{\bullet}OH$) and perhydroxyl radicals ($HO_2^{\bullet}$), which are the major reactive species generated via the catalytic decomposition of H_2O_2.

Similar behaviorwas largely reported in the literature. D.E. Shahwar et al. [61], S.B. Hammouda al. [24,25], Y. Liu et al. and Xu et al. [62,63], Karale et al. [64] reported the negligible reactivity of hydrogen peroxide alone towards dyes, indolic, phenolic and pharmaceutical compounds [64], respectively. E. Neyenes et al. [65] have reported in their review that although H_2O_2 is thermodynamically a strong oxidant Eqs. (2)Eqs. (3) (standard potential 1.80 and 0.87 V at pH 0 and 14, respectively), the oxidation by H_2O_2 alone at reasonable concentrations is not effective for most refractory contaminants because of low rates of reaction so that activation by using transition metals is required.

$$H_2O_2 + 2H^+ + 2e- \rightarrow 2H_2OE^\circ = 1.77V(2)$$

$$HO_2^- + H_2O + 2e- \rightarrow 3OH^-E^\circ = 0.87V(3)$$

The adsorption of BPF molecules on the envisaged catalysts was also investigated. In the adsorption phase, adsorption equilibrium was quickly reached and only physical adsorption was observed for the different samples. The adsorption capacities of CeO_2, $LaCuO_3$, CeO_2LaCuO_3 and CeO_2-$LaFeO_3$were 15.53%, 8.29% and 7.48%, 11.78 and 10.41 for bisphenol F, respectively. CeO_2-$LaMO_3$ exhibited

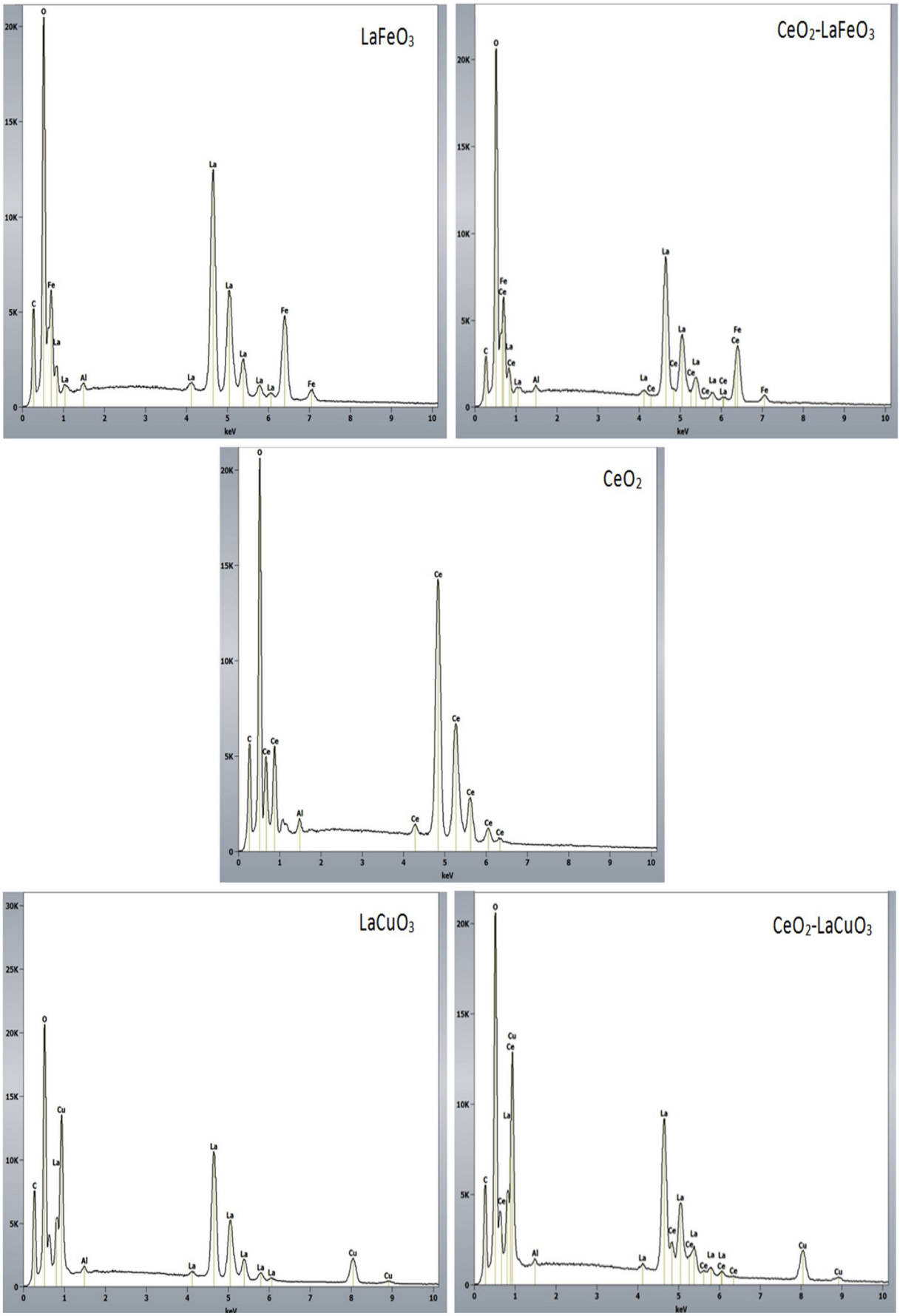

Fig. 3. Energy dispersive X-ray spectroscopy (EDS) spectra acquired in scanning electron microscopy (SEM) at the top view samples of CeO_2, $LaFeO_3$, $LaCuO_3$, CeO_2-$LaFeO_3$ and CeO_2-$LaCuO_3$. Acc voltage 15Kv, Scale bars are 5 μm.

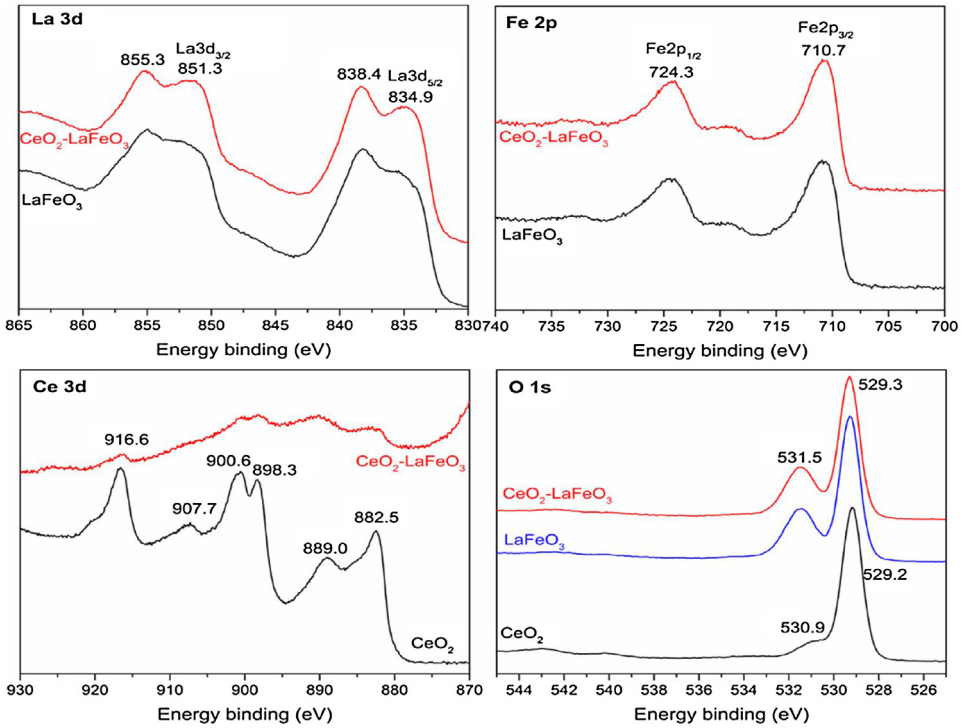

Fig. 4. XPS spectra of La 3d, Fe 2p, Ce 3d, and O 1s for $LaFeO_3$, CeO_2 and CeO_2-$LaFeO_3$.

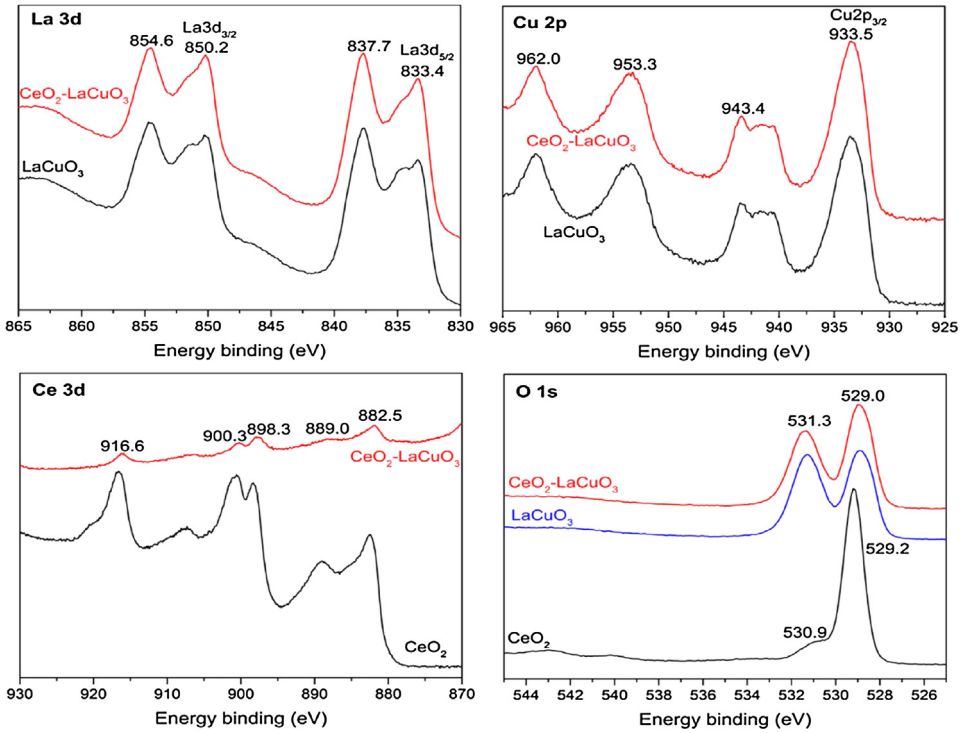

Fig. 5. XPS spectra of La 3d, Cu 2p, Ce 3d, and O 1s for $LaCuO_3$, CeO_2 and CeO_2-$LaCuO_3$.

much higher adsorptive ability than $LaMO_3$, which was ascribed to the larger surface areas of CeO_2-$LaMO_3$.

Subsequently, the catalytic degradation of BPF, in the presence of oxidant, at pH 3 was investigated. Fig. 6-shows the comparisons of time-dependent reaction yields between the five catalysts. The different catalysts had substantially different performances in the catalytic oxidation of BPF. The perovskite-ceria composites exhibit greater catalytic performance for BPF degradation than did the pure perovskite and ceria nanoparticles, implying that the catalytic activity was enhanced by the introduction of ceria. CeO_2-$LaCuO_3$ had the highest activity.

Fig. 6b summarizes the results of kinetic analysis for the various nanocrystals. The degradation of BPF was found to follow a pseudo first order kinetics model. This result is consistent with

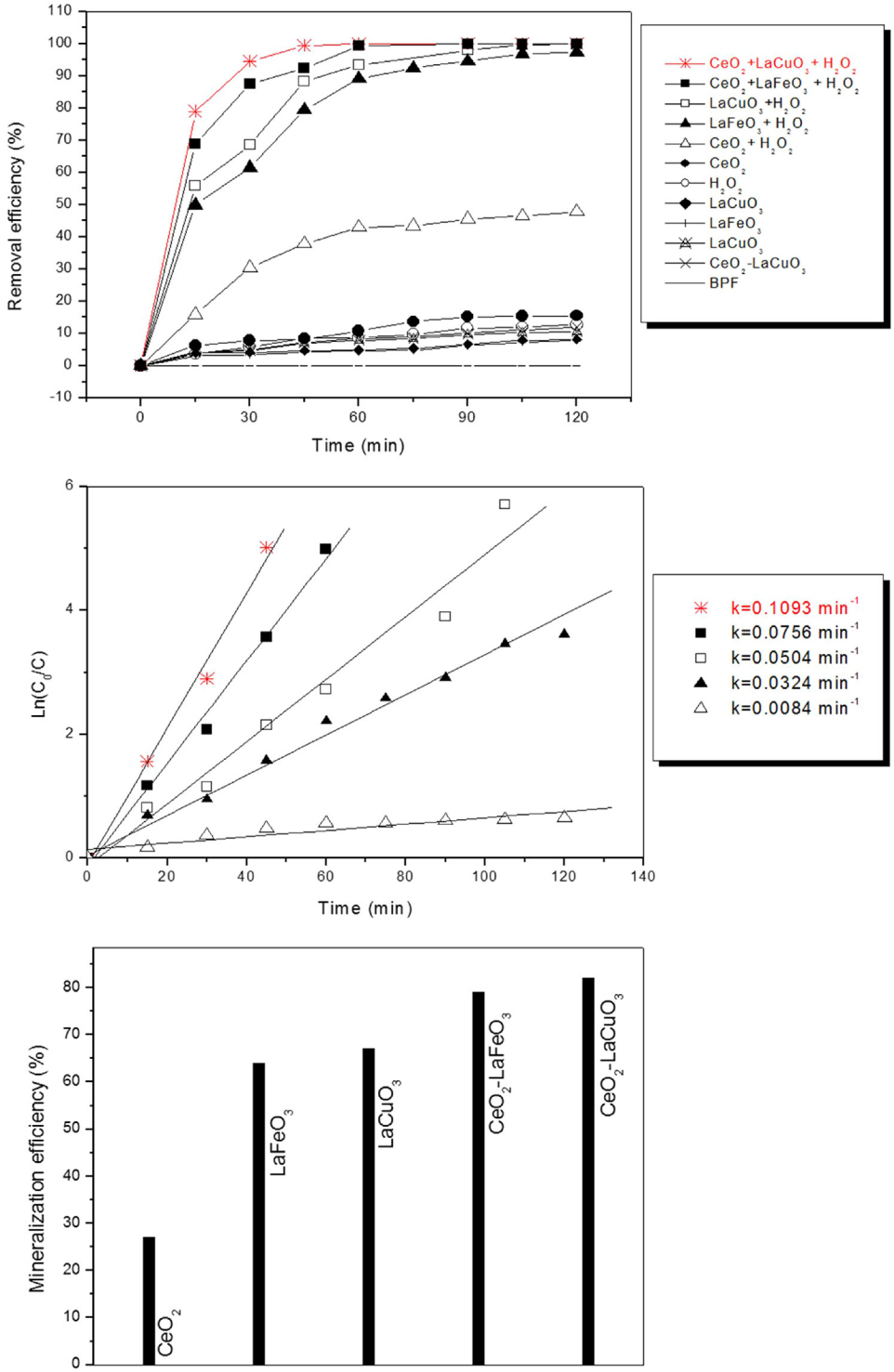

Fig. 6. Adsorptive behavior of bisphenol F (Experimental conditions: Catalyst loading 0.2 gL^{-1}, pH = 3), [Bisphenol F]$_0$ = 20 mg L^{-1}, working volume = 100 mL, and its degradation behavior under H_2O_2/Catalyst system (Experimental conditions: [H_2O_2] = 10 mM, Catalyst loading 0.2 g L^{-1}, pH = 3, working volume of 100 mL, [Bisphenol F]$_0$ = 20 mg L^{-1}) (b) Kinetic behavior under the heterogeneous Fenton system, (c) Mineralization of Bisphenol F solutions with various catalyst.

the idea that the degradation reaction of organic compound by Fenton process obey second-order kinetics and that the generated hydroxyl radical OH• reaches a steady state after a certain operation time [67,24]. After 45 min of reaction, the BPF removal efficiency reached 100, 92.34, 88.34, 81.83 and 37.88% for LaCuO3-CeO_2, $LaCuO_3$, $LaFeO_3$, $LaFeO_3$-CeO_2 and CeO_2, respectively. The corresponding rate constants (kapp) were 0.1093, 0.0756, 0.0504, 0.0324 and 0.0084 min^{-1}, respectively (Fig. 6b).

The oxygen mobility and the redox property of the ceria appear to be responsible for the higher catalytic activity of the composite catalysts. In fact, the substitution of cerium species with transition metal produces a contraction of the cell volume and induces stress in the structure and consequently structural defects that increase the oxygen mobility.

Comparative experiment was conducted by a physical mixture of $LaCuO_3$ and CeO_2 nanoparticles with hydrogen peroxide. Com-

plete removal of bisphenol F was reached after 120 min (data not shown). The catalytic activity of Perovskite-Ceria composite was higher than that of mixture materials, thereby improving the relative rates of mass transfer to reactive sites and chemical reaction at reactive sites. Similar observation was reported by Xu et al. [66] in their investigation of the heterogeneous Fenton degradation of 4-Chlorophenol by the magnetic nanoscaled Fe_3O_4/CeO_2 composite.

The noticeable reactivity of pure cerium oxide could be attributed to its capacity to decompose hydrogen peroxide, as reported in several studies. This activity is related to the ceria ability in providing surface active sites and correlated as well to its oxygen storage and release capacity through the redox shift between Ce^{4+} and Ce^{3+} under oxidizing and reducing conditions, respectively.

In this study, it is worth noting that the reaction between ceria and hydrogen peroxide induces a visual color change in the CeO_2 nanoparticle color from light yellow to a dark orange-brown which indicate the formation of peroxide-species ($=Ce^{3+}$-OOH^-). These species inhibit the Fenton like cycle which can explains the limited performance of ceria oxide in comparison with the others catalysts. According to the XPS results, more Ce^{3+} are formed in the perovskite-ceria catalysts. Thus, during the treatment, we can suggest an enhancement of ceria reduction from Ce^{4+} to Ce^{3+} by an electron transfer from the transition metal to the CeO_2 in the composite structure. Consequently, more reactive oxygen species were generated via the interaction of hydrogen peroxide with Ce^{3+}, which is in favor of the Fenton like degradation of bisphenol F.

The catalysis activity of pristine $LaCuO_3$ was observed higher than that of pristine $LaFeO_3$. According to the previous reports, the surface Cu(II) species could complex with phenol and its intermediates via σ bonding and π → Cu(II) interaction. The resulted Cu(II)-phenoxo complexes was reported to cause the reduction of Cu(II) to Cu(I) and facilitate the decomposition of H_2O_2 to generate more hydroxyl radicals [68], resulting in better catalysis efficiency of $LaCuO_3$ than $LaFeO_3$, where Fe(III)-phenoxo complexes has not been reported in our best knowledge.

4. Catalysts stability

In the application of heterogeneous catalysts,special attention should be paid to the catalyst stability and reusability. The catalyst deactivation which is associated with metal leaching is considered as the major disadvantage of heterogeneous catalysis. Furthermore, the homogeneous contribution of dissolved metals may distort the interpretation of the obtained results. To investigate the stability of the perovskite catalysts with respect to metal leaching, the concentrations of dissolved Fe and Cu metals after reaction were analyzed by using ICP (Fig. 7). At pH 3, it was found that 1.28 mg L^{-1} Fe and 0.98 mg L^{-1} Cu were leached in the cases of pristine $LaFeO_3$ and $LaCuO_3$, respectively, but no detectable amount of dissolved Fe and Cu metals could be measured for the corresponding perovskites coupled with CeO_2. Accordingly the addition of CeO_2 significantly enhanced the stability of the catalysts. For all the catalysts, the amount of leached cerium was below detection limit (<0.01 mg L^{-1}). Slightly higher levels of lanthanum leaching were determined (1.89, 1.78, 0.77, 0.36 mg L^{-1} for $LaFeO_3$, $LaCuO_3$, CeO_2-$LaFeO_3$ and CeO_2-$LaCuO_3$, respectively). The relatively satisfactory stability of the pristine perovskites is consistent with data reported by Sotelo et al. who studied the catalytic wet peroxide oxidation of phenolic solutions over a $LaTiCuO_3$ perovskite catalyst [68]. The enhancement of perovskites stability after ceria introduction can be explained in terms of the following reasons.

The standard reduction potential of Ce^{4+}/Ce^{3+} is 1.61 V, while those of Fe^{3+}/Fe^{2+} and Cu^{2+}/Cu^{+} are 0.77 and 0.15 V, respectively

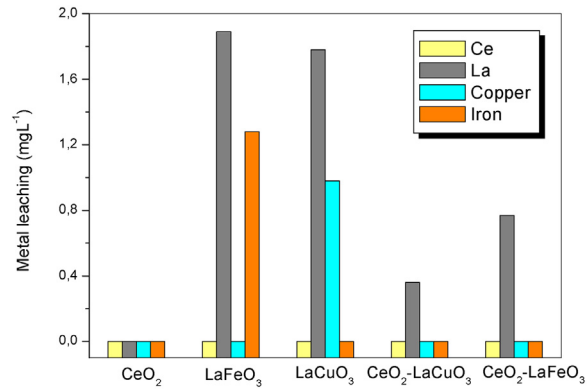

Fig. 7. Evaluation of catalyst stability:total metals leached amounts after 2 h of treatment (Experimental conditions: $[H_2O_2]$ = 10 mM, Catalyst loading 0.2 g L^{-1}, pH=3, working volume of 100 mL, $[\text{Bisphenol F}]_0$ = 20 mg L^{-1}).

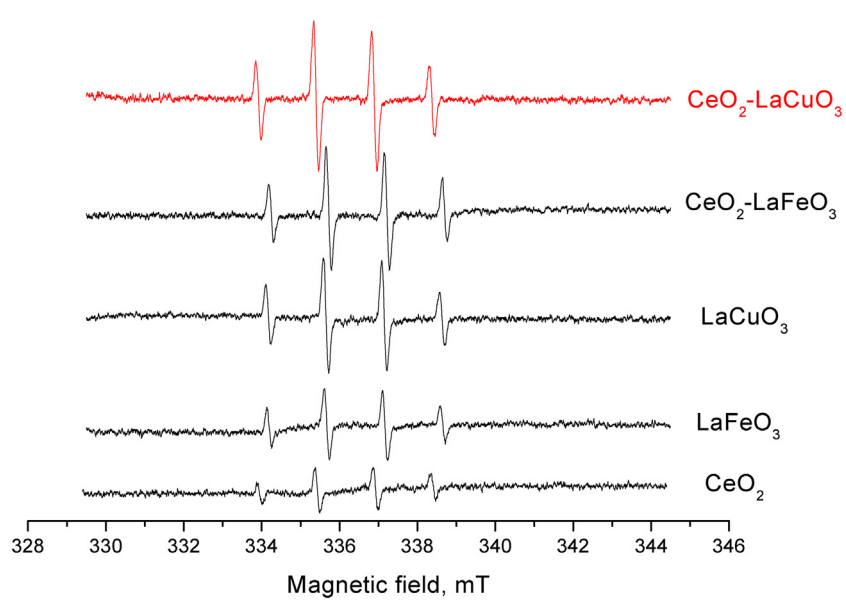

Fig. 8. DMPO spin trapping ESR spectra recorded at pH 3 in aqueous dispersion with the five as-prepared catalysts.

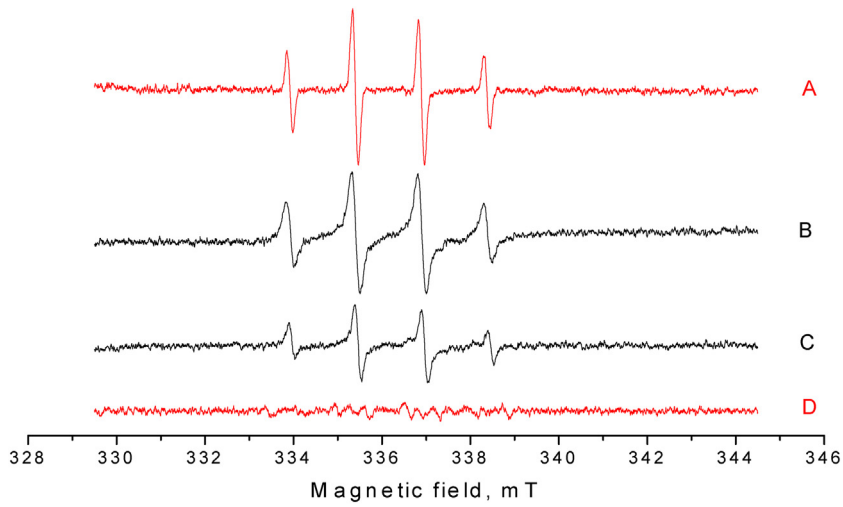

Fig. 9. ESR spectra of (CeO_2-$LaCuO_3$/H_2O_2/DMPO) mixture recorded at pH 3 (A) in aqueous dispersion for DMPO-•OH and (D) in methanol dispersion for DMPOHO_2•/O_2•−. ESR spectra of (CeO_2-$LaCuO_3$/H_2O_2/DMPO) mixture recorded at pH 7 after addition of Bisphenol F (B) and without addition of bisphenol F (C).

[69]. Thus the electron transfer from $\equiv Fe^{2+}$Eq. (4) and $\equiv Cu^{+}$ Eq. (5) to $\equiv Ce^{4+}$ could be thermodynamically spontaneous as following:

$$\equiv Fe^{2+} + \equiv Ce^{4+} \rightleftharpoons \equiv Fe^{3+} + \equiv Ce^{3+} (4)$$

$$\equiv Cu^{+} + \equiv Ce^{4+} \rightleftharpoons \equiv Cu^{2+} + + \equiv Ce^{3+} (5)$$

According to the XPS results, the states of iron and copper are Fe(III) and Cu(II), hence the addition of CeO_2 could facilitate the recycle of the dissolved Fe^{2+} and Cu^{+} into Fe^{3+} and Cu^{2+} species in the perovskite catalysts, thus reducing the leaching of these metal elements. Similar recycling behavior has also been reported in the Fe_3O_4/CeO_2 Fenton-link catalyst system by Xu et al. [66]. More importantly, the resulted $\equiv Ce^{3+}$ can cause oxygen vacancies on the surface of CeO_2, further enhancing the defect sites and improving the catalytic activity. This could explain the behavior that the addition of CeO_2 could enhance the degradation efficiency of $LaFeO_3$ and $LaCuO_3$. Moreover, after CeO_2 addition, the increase of the activity of $LaCuO_3$ was more significant in comparison with $LaFeO_3$. This could due to the fact that the redox potential difference between Ce^{4+}/Ce^{3+} and Cu^{2+}/Cu^{+} (1.46 V) is much higher than that between Ce^{4+}/Ce^{3+} and Fe^{3+}/Fe^{2+} (0.84 V). Hence, the electron transfer from $\equiv Cu^{+}$ to $\equiv Ce^{4+}$ could be more thermodynamically favored than that from $\equiv Fe^{2+}$ to $\equiv Ce^{4+}$.

5. Evaluation of catalysts performance in terms of mineralization efficiency

For industrial wastewater applications, the catalyst potential must be evaluated mainly in terms of its mineralization performance. Thus, the investigation of mineralization degree for bisphenol F was additionally performed under prolonged treatment (6 h) with TOC removal measurements. In agreement with the changes of bisphenol F concentration found above, ceria-perovskite composites nanoparticles presented much higher activity than pristine perovskites in Bisphenol F mineralization. The mineralization efficiencies were observed to decrease in the order of CeO_2-$LaCuO_3$ (82.43%)> CeO_2-$LaFeO_3$(78.39%)> $LaCuO_3$(67.42%) > $LaFeO_3$(63.87%) > CeO_2(27.79%). From the incomplete mineralization, it could be speculated that the BPF degradation produce some intermediates which were refractory to the Fenton-like reaction, thus they cannot be entirely mineralized in 6 h. This point will be discussed in detail subsequently. In summary, we can conclude that using transition metals in combination with cerium induces synergetic effect on BPF removal. Considering their high stability and performance, the next catalytic experiments were carried out over the ceria doped perovskite catalysts.

Mechanism of the heterogeneous reaction

The Fenton heterogeneous system for reactive radicals' generation is a surface controlled process which depends mainly on H_2O_2 concentration and the catalyst properties. The bisphenol F oxidation involves firstly the surface adsorption of BPF molecules onto the composite surface through electrostatic interaction and π-π stacking. Likewise, hydrogen peroxide is instantaneously adsorbed onto the catalyst surface and its breakage leads to the generation of powerful oxidizing species which react with BPF molecules in solution and initiate the oxidative reaction.

To ascertain the catalytic reaction mechanism, (EPR) was employed in order to probe the (ROS) produced on the catalysts surface and to explore the effect of ceria doping on the radicals generation.The formation of hydroxyl radicals (•OH) was verified by EPR spectroscopy using 5,5-dimethyl-1-pyrrolidoneN-oxide (DMPO) as a spin-trapping system specific of •OH. DMPO reacts with •OH to generate a relatively stable nitroxyl radical [70].

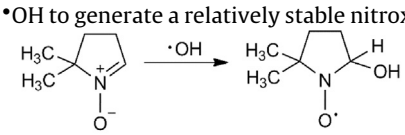

DMPC **Stable radical adduct**

For all the investigated catalysts, a quartet with a symmetrical 1:2:2:1 signal intensity was detected, which is in good accordance with the pattern reported by for the DMPO-OH adduct, confirming that hydroxyl radicals are the dominant active species responsible for BPF removal in the heterogeneous Fenton/system. •OH production in the complete reaction mixture was dependent on the presence of catalyst and did not occur when H_2O_2 alone was added to the solution.

Examination of Fig. 8 shows that •OH radicals were generated for the five samples and the main difference between them was as predicted in the intensity of the DMPO/•OH signal which follows the trend: $LaCuO_3$-CeO_2 > $LaFeO_3$-CeO_2 > $LaCuO_3$ > $LaFeO_3$ > CeO_2. The intensity of the generated hydroxyl radicals was found to be almost 4 times higher for $LaCuO_3$-CeO_2 than for ceria alone. These results were consistent with the observed enhancement in BPF removal.

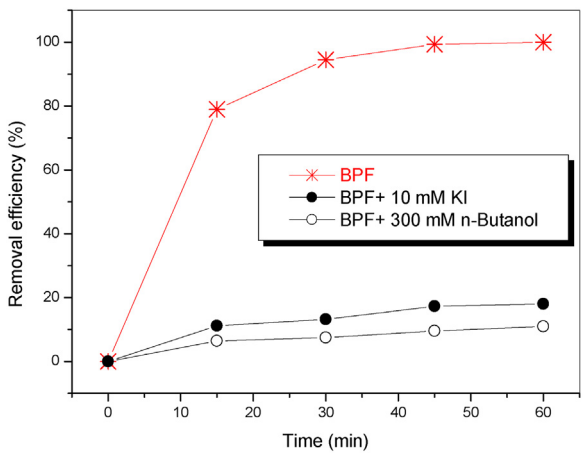

Fig. 10. Effect of Radicals scavengers on BPF degradation (Experimental conditions: $[H_2O_2] = 10$ mM, CeO_2-$LaCuO_3$ loading 0.2 g L^{-1}, pH = 3, working volume of 100 mL, $[\text{Bisphenol F}]_0 = 20$ mg L^{-1}; T = 25 °C).

Moreover, since the $HO_2^{\bullet}/O_2^{\bullet-}$ radicals in water are known to be very unstable and underwent easy disproportionation rather than slow reaction with DMPO, their formation possibilities was herein investigated by methanol addition to the catalysts (Fig. 9D). Instead of ultrapure water, methanol was used as a reaction medium to extend the half-life of $O_2^{\bullet-}$. However, the sextet characteristic peaks of DMPO—$O_2^{\bullet-}$ were not observed, which suggest that hydrogen peroxide was mostly decomposed into hydroxyls radicals.

To further confirm that the dominantreactive entities produced during the activation of hydrogen peroxide by the based perovskite catalysts are hydroxyl radicals, quenching tests was performed with CeO_2-$LaCuO_3$ catalyst using *n*-butanol as scavenger of all the hydroxyl radicals produced in the CeO_2-$LaCuO_3/H_2O_2$ system (both surface-bounded •OH and free •OH). As can be seen from Fig. 10, the degradation of BPF was inhibited greatly by the addition of excess *n*-butanol (300 mM) (decrease to 11%) which confirms that OH radicals are the major reactive oxygen species generated in the envisaged system.

Iodide ion is commonly used as a scavenger that can react quickly with the hydroxyl radicals produced at the catalyst surface. As seen in Figure, adding excess KI (10 mM) led to a considerable decrease in the BPF removal efficiency from 100% to 18%, indicating that surface-bounded OH was the major species among the hydroxyl radicals responsible for the removal of Bisphenol F.Therefore, about 7% and 82% BPF removal might be ascribed to the action of free •OH, and surface-bounded OH, respectively. Thus, about 11% removal of BPF might be attributed to the action of other oxygen reactive species ($HO_2^{\bullet}/O_2^{\bullet-}$).

The dominance of the surface-bounded •OH might be explained by the weak polarity of BPF molecules which ensures their adsorption on the catalyst surface. Thus the BPF degradation primarily occurred on the boundary between the solid phase and liquid phase. Therefore, a possible reaction mechanism of bisphenol F oxidation and removal in CeO_2-$LaMO_3$ (M = Fe, Cu) Fenton-like system was proposed and schematized in Fig. 11.

The mechanism for hydrogen peroxide decomposition in the presence of water-oxide interfaces is still not completely elucidated, but it was suggested that it occurs on the surface with the hydroxyl and peroxy radicals' generation. On the catalyst surface, $\equiv M^{n+1}$ could react with hydrogen peroxide to produce peroxyhydroxyl radicals $HO^{\bullet}{}_2$ Eq. (6) which in turn reacts with $\equiv M^{n+1}$ to produce $\equiv M^{n+}$ Eq. (7)and initiate the Fenton –like reaction producing the surface-bound hydroxyl radicals ($^{\bullet}OH_{ads}$) Eq. (8). The standard reduction potential of Ce^{4+}/Ce^{3+} is 1.44 V, while that of Fe^{3+}/Fe^{2+} is 0.77 and Cu^{2+}/Cu is 0.34 v, respectively;hence, the electron transfer from $\equiv Fe^{2+}$ or $\equiv Cu^{+}$ to $\equiv Ce^{4+}$ Eq. (12) is thermodynamically favored. In the presence of hydrogen peroxide and behaving similarly to metal transitions in a Fenton-like reaction, cerium species are capable of redox cycling and $^{\bullet}OH_{ads}$ radicals formation, as shown in Eqs. (13). Similarly to the ≡M entities, the ≡Ce entities would be recycled on the ceria-perovskite composite. A minimal amount of the generated $^{\bullet}OH_{ads}$ radicals could also enter to the bulk solution through diffusion effect. The adsorbed and free radicals can then oxidize the bisphenol F molecules present at the surface catalyst and in the bulk solution, respectively.

$$\equiv M^{n+1} + H_2O_2 \rightarrow \equiv M^{n+} + H^+ + HO^{\bullet}{}_2 \quad (6)$$

$$\equiv M^{n+1} + HO_2^{\bullet} \rightarrow \equiv M^{n+} + H^+ + O_2 \quad (7)$$

$$\equiv M^{n+} + H_2O_2 \rightarrow \equiv M^{n+1} + OH^- + OH^{\bullet}{}_{ads} \quad (8)$$

$$OH^{\bullet} + H_2O_2 \rightarrow HO_2^{\bullet} + H_2O \quad (9)$$

$$\equiv M^{n+} + HO_2^{\bullet} \rightarrow \equiv M^{n+1} + HO_2^- \quad (10)$$

$$\equiv Ce^{4+} + \equiv M^{n+} \rightarrow \equiv Ce^{3+} + \equiv M^{n+1} \quad (12)$$

$$\equiv Ce^{3+} + H_2O_2 \rightarrow \equiv Ce^{4+} + OH^- + OH^{\bullet} \quad (13)$$

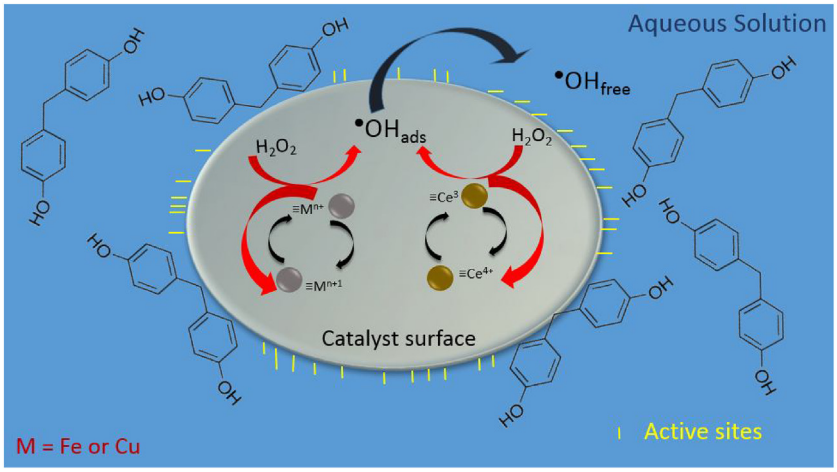

Fig. 11. Schematic presentation of the main reaction mechanism involved in the oxidation of Bisphenol F by the heterogeneous perovskite based catalyst.

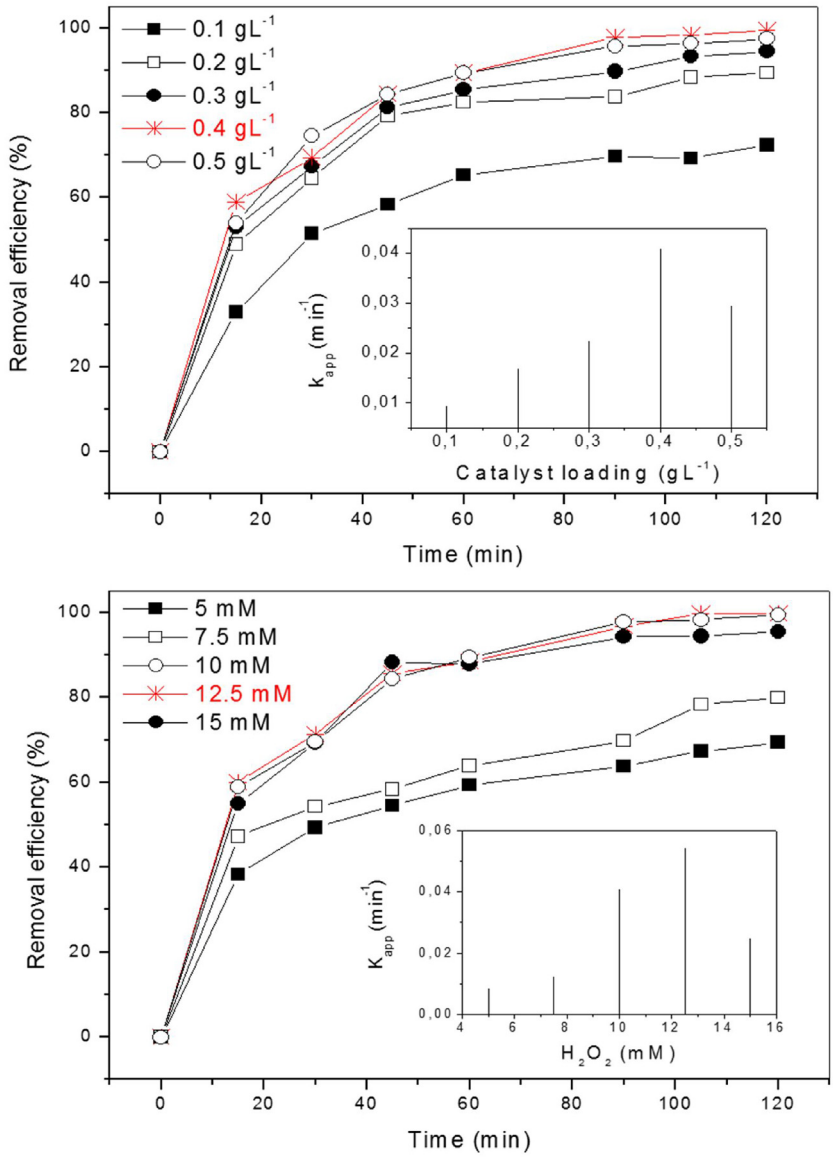

Fig. 12. Influence of catalyst dosage ([H_2O_2]: 10 mM)and oxidant concentration ([CeO_2-$LaCuO_3$]: 0.4 g L^{-1}) on the heterogeneous Fenton like degradation of bisphenol F. Experimental conditions: working volume of 100 mL, $[BPF]_0$: 20 mg L^{-1}; pH: 7.0; T = 25 °C.

6.7. Bisphenol F oxidation at neutral conditions (pH 7)

It is well known that most wastewater effluents have neutral or near neutral pH. Consequently, acidic conditions induces high cost of chemicals needed for acidifying effluents before treatment and subsequently neutralizing them before discharge [71]. Thus, from a practical and economical point of view, it is necessary to assess the possible reactivity of the ceria-perovskite composites CeO_2-$LaFeO_3$ and CeO_2-$LaFeO_3$ at neutral conditions.

We revealed that the increase in solution pH from 3 to 7 affected negatively the catalytic efficacy of the catalysts. A considerable decrease in the bisphenol F concentration was only observed over $LaCuO_3$-CeO_2 catalyst. After a reaction time of 2 h, the BPF removal efficiency doesnot exceed 30% over $LaFeO_3$-CeO_2(data not shown). For CeO_2-$LaFeO_3$ the signal of DMPO-•OH adduct is very weak (data not shown), suggesting its low catalytic activity for the activation of H_2O_2 at pH 7. These results are in accordance with the literature. In their interesting review of iron Fenton-like systems for activating H_2O_2 in advanced oxidation processes, Bokare et al. [72] reported that the Cu^{2+}/H_2O_2 Fenton like process should work over a broader pH range, compared to the Fe^{3+}/H_2O_2 redox system working only in acidic conditions. According to their review, various copper based Fenton catalysts efficiently generate hydroxyl radical for the oxidation of several organic compounds in near neutral or neutral aqueous medium.

EPR analysis confirmed the reactivity of the copper based perovskite catalyst at neutral conditions. As depicted in Fig. 9, at pH 7, the four characteristic peaks of DMPO-•OH were observed in the suspension of $LaCuO_3$-CeO_2 with H_2O_2 (Fig. 9C). Moreover, It isworth noting that the intensity of the DMPO-OH adduct signal significantly increased in the presence of BPF molecules (Fig. 9D). In view of these observations, it can be speculated that the interaction between the catalyst and BPF promoted the decomposition of hydrogen peroxide into hydroxyl radicals. Interestingly, the interaction of H_2O_2 with the surface Cu(II) species of $LaCuO_3$-CeO_2 could produce phenoxo-Cu(II) complexes with BPF and its intermediate which could cause the interaction of the organic ligand part with the activated H_2O_2. According to the interesting work of Zhang et al. [69] devoted to the degradation of bisphenol A using the framework Cu-doped $AlPO_4$ as Fenton-like catalyst, Cu(II) in the

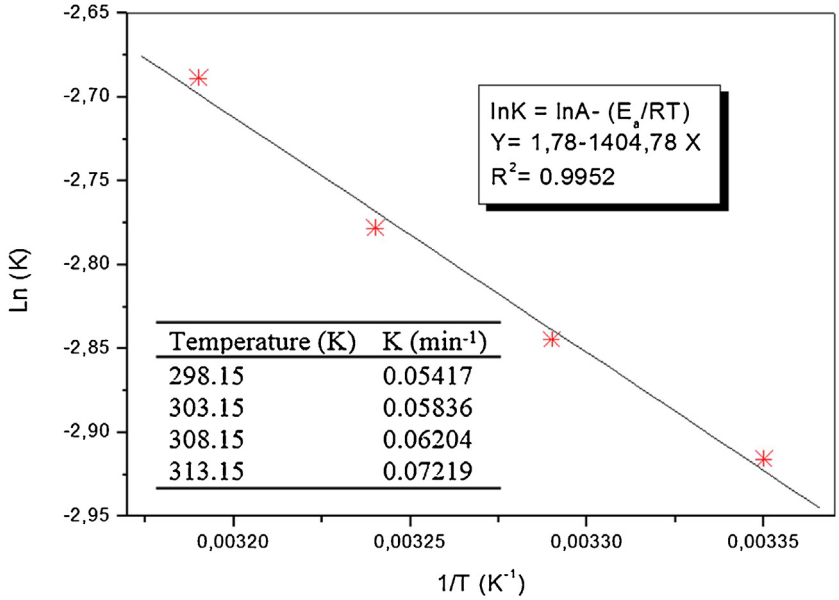

Fig. 13. Arrhenius-type plot of the apparent pseudo first order kinetic constants.

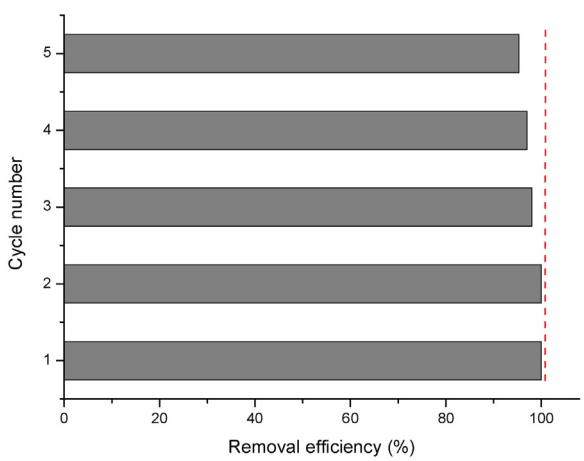

Fig. 14. Bisphenol F oxidation on CeO_2-$LaCuO_3$ catalyst in five consecutive runs.

phenoxo-Cu(II) complexes would get an electron due to the charge transfer from the benzene ring to Cu(II) by the $\pi \rightarrow$ Cu(II) interaction, leading to the reduction of Cu(II) to Cu(I) and the accelerated decomposition of H_2O_2 into more OH on the catalyst surface, resulting in the high activity of $LaCuO_3$-CeO_2 [69]. A similar observation was highlighted by Zhang et al. [73] during the phenol hydroxylation by copper-containing MCM-41 mesoporous silicas catalysts. The interaction of hydrogen peroxide with the copper-oxo species has been reported to produce a CuOOH intermediate which can react further with hydrogen peroxide to produce hydroxyl radicals.

To acquire an in-depth understanding of the Fenton –like catalyst CeO_2-$LaCuO_3$, the influence of the main experimental conditions on its reactivity at pH 7 will be discussed in the following sections.

7. Catalyst loading effect

The removal of bisphenol F in the Ceria-$LaCuO_3$ Fenton-like system was studiedusing different catalyst amounts. As depicted in Fig. 12, the catalytic removal efficiency of BPF increased from 72.43 to 99.12% as the catalyst concentration increased from 0.1 to 0.4 g L^{-1}. The kinetic apparent constant increased from 0.0093 to 0.0408 min^{-1}. The improvement of the catalytic performance could be ascribed to the increasing of available active sites for BPF adsorption and •OH production. A slight decrease was observed for catalyst loading >0.4 gL^{-1}, which is possibly related to the self-scavenging effect of hydroxyl radicals by excess of M^{n+} (M=Ce, Cu) Eq. (15). This trend can be also related to the agglomeration of nanoparticles.

$$^{\bullet}OH + \equiv M^{n+} \rightarrow OH^{-} + M^{n+1} \quad (15)$$

Obviously the degradation rate constant increased from 0.0083 to 0.0054 min^{-1} as the hydrogen peroxide dosage increased from 5 to 10 mM. H_2O_2 is the precursor in the reaction with the metal transition (M^{n+}) producing hydroxyls radicals according to the classical Haber-Weiss mechanism, and it can also react with M^{n+1} to regenerate the M^{n+} state that can participate in the Fenton-like reaction. Nevertheless, with a higher H_2O_2 loading (15 mM), the rate constant decrease to 0.0247 min^{-1}, which is probably due to the scavenging effect of H_2O_2 Eq. (16).

$$^{\bullet}OH + H_2O_2 \rightarrow H_2O + HO_2^{\bullet} \quad (16)$$

The kinetics of Bisphenol F oxidation was also evaluated at various temperatures (25, 30, 35, and 40 °C). As expected, the BPF removal performance was enhanced with increasing temperature. The reaction rate constants were 0.054, 0.058, 0.062 and 0.072 min^{-1} at 25, 30, 35 and 40 °C respectively. The activation energy Ea of the reaction on the CeO_2-$LaCuO_3$ surface was determined by plotting lnK against 1/T (Fig. 13) on the basis of the Arrhenius equation Eq. (17) and was determined as 11.659 KJ mol^{-1}. This value is indicative of a diffusion-controlled reaction which is usually characterized by smaller activation energy, typically 10–13 kJ mol^{-1}, indicating that the reaction rate for this heterogeneous system is dominated by the rate of mass transfer rather than the intrinsic reaction rates on the surface of the ceria-perovskite catalyst.

$$k = A\exp(-E_a/RT) \quad (17)$$

Where, A is the Arrhenius constant, Ea (kJ mol^{-1}) is the apparent activation energy, R is the ideal gas constant (0.0083 K J mol^{-1} K^{-1}), and Tis the solution temperature in K.

The oxidative degradation of organic compounds must continue unto the quasi-complete mineralization of the treated solution. Table 3 summarizes the mineralization degrees obtained from the

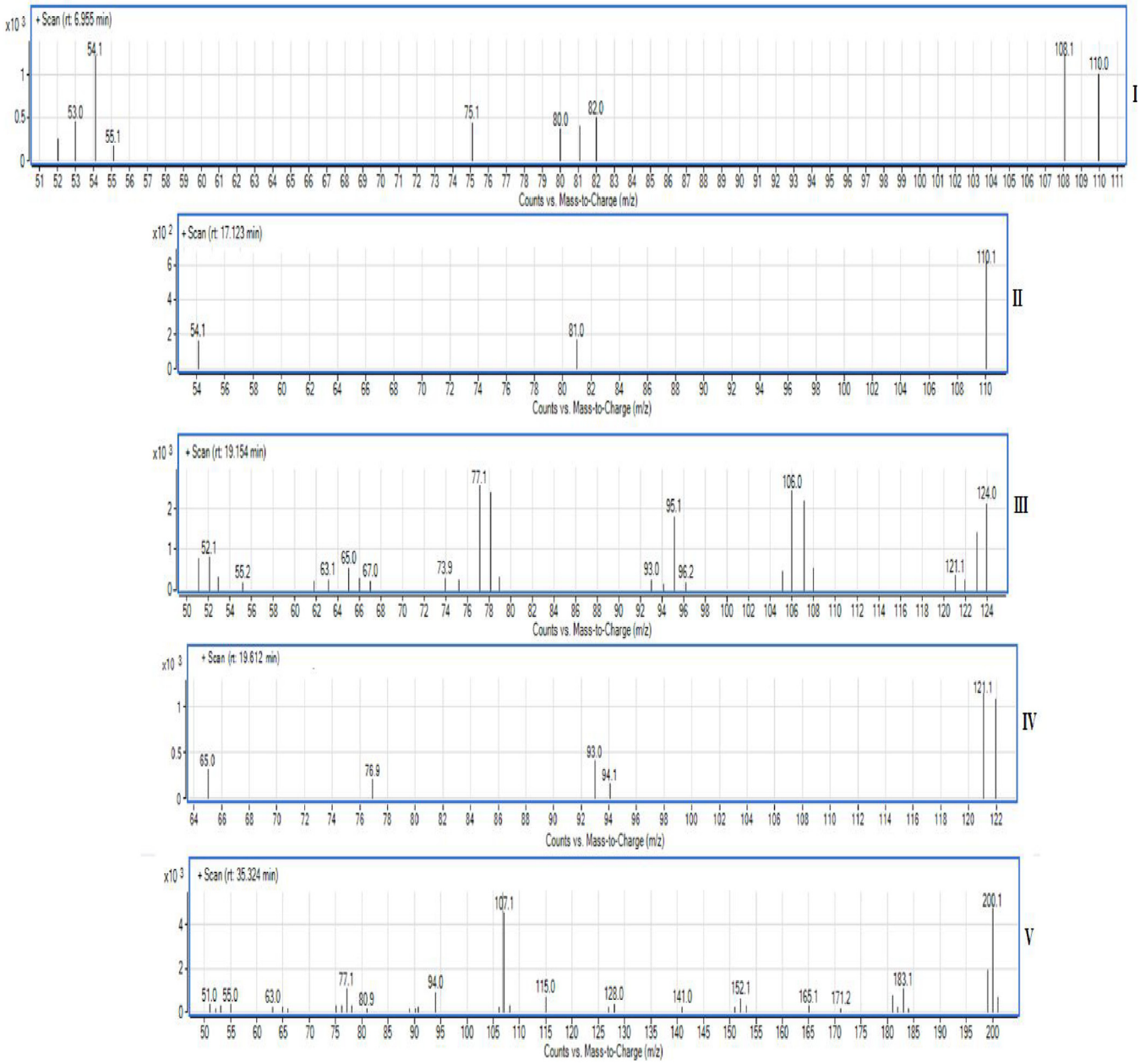

Fig. 15. Mass spectrum of the Bisphenol F degradation intermediate, I-V correspond to those listed in Table.

Table 3
Bisphenol F and TOC removal efficiencies recorded at pH 7 under various operational conditions.

Temperature (°C)	catalyst dosage mg L^{-1}	H_2O_2 mM	BPF removal (%)	Kinetic rate (min^{-1})	TOC removal (%)
25	0.1	10	72.52	0.00929	48.77
25	0.2	10	89.11	0.01677	59.01
25	0.3	10	94.23	0.0223	65.12
25	0.4	10	99.49	0.04084	71.18
25	0.4	5	69.43	0.00827	49.93
25	0.4	7.5	79.93	0.01236	58.09
25	0.4	12.5	99.85	0.05414	72.44
30	0.4	12.5	100	0.05836	73.07
35	0.4	12.5	100	0.06203	77.18
40	**0.4**	**12.5**	**100**	**0.07410**	**82.03**

various operating conditions after 6 h of treatment under neutral conditions. As could be observed, the highest TOC removal percentage (≈82%) was obtained at 40 °C, 0.4 gL^{-1} CeO_2-$LaCuO_3$ and 12.5 mMH_2O_2. Quasi-total mineralization of the Bisphenol F solutions (95%) was achieved after 12 h of treatment under optimized conditions of catalyst/H_2O_2 system, showing that BPF and its intermediates were nearly completely mineralized to CO_2 and water.

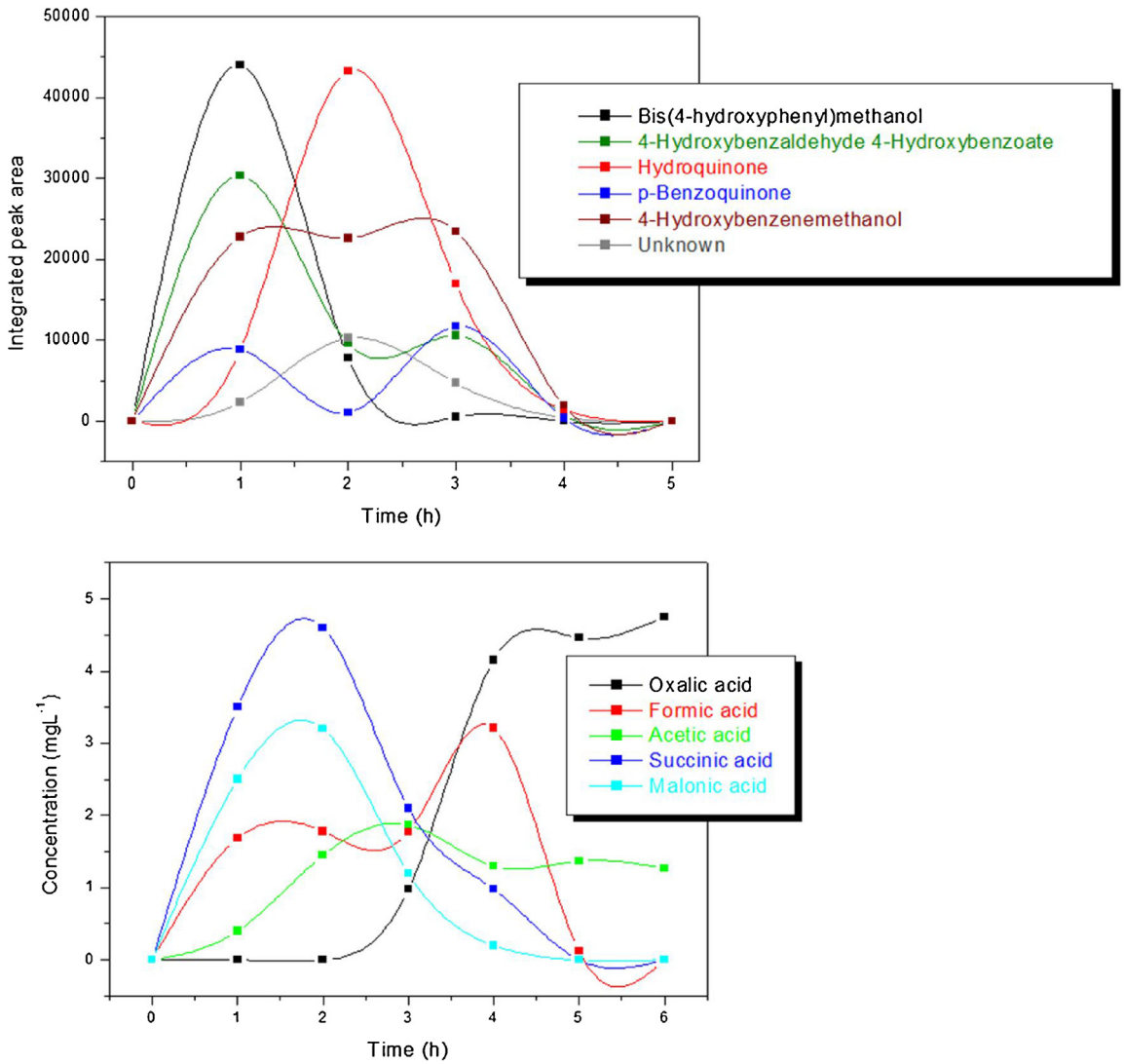

Fig. 16. Time–course of bisphenol F derivatives during the degradation of 200 mg L^{-1} BPFaqueous solution. Experimental conditions: $[BPF]_0$: 200 mg L^{-1}; $[CeO_2\text{-}LaCuO_3]$: 0.4 g L^{-1}; $[H_2O_2]$: 12.5 mM; pH: 7.0.

In summary, ceria doped copper perovskite could be considered as an interesting catalyst that provides efficient oxidative degradation of bisphenol F and a relatively high TOC removal values at neutral conditions and moderate oxidant concentration, thus resulting in significant cost savings.

8. Determination of the absolute rate constant

The absolute rate constant of the reaction between Bisphenol F and hydroxyl radicals during the Fenton oxidation was determined by the competition kinetics method using benzoic acid (BA) as a well-known standard competitor, since its absolute rate constant is well established as $K_{BA} = 4.3 \times 10^9\ M^{-1}\ s^{-1}$ [74–76]. For this purpose, competitive kinetic experiment was performed with both compounds in equal concentration (20 mg L^{-1}).

Assuming a pseudo-first order kinetic for both BPF and BA reactions with hydroxyl radicals, apparent rate constant values of BPF and BA were then determined as 0.036 and 0.074 min^{-1}, respectively. The absolute rate constant (k_{abs}) was calculated by means of Eq. (14):

$$k_{abs(BisphenolF)} = k_{abs(BA)} \frac{k_{app(BisphenolF)}}{k_{app(BA)}} \quad (18)$$

The absolute rate constant of the reaction between Bisphenol F and hydroxyl radicals was determined as $2.0910^9\ M^{-1}\ s^{-1}$. No value of absolute rate constant for the hydroxylation of bisphenol F was found in the literature for comparison.

9. Stability

Catalyst recyclability and stability are two of the key factors for industrial applications. In order to make the $CeO_2\text{-}LaCuO_3$ catalyst more attractive to be used on a large scale, the composite material must have the capacity to be regenerated and reused again.

The removal efficiency of bisphenol F obtained with the regenerated heterogeneous catalyst for consecutive runs is reported in Fig. 14. After each run of reaction, the catalyst was centrifuged out, washed with distilled water and then re-dispersed into 100 mL of the new BPF aqueous solution with the initial concentration (20 mg L^{-1}). The results showed that Bisphenol F removal remained almost constant for four cycles of reuse. The slight decrease (~5%) observed from the five cycle could be ascribed to the deactivation of some catalyst sites by adsorption of some intermediates over the surface catalyst. A similar trend was reported by other studies and they came up with the conclusion that the presence of resid-

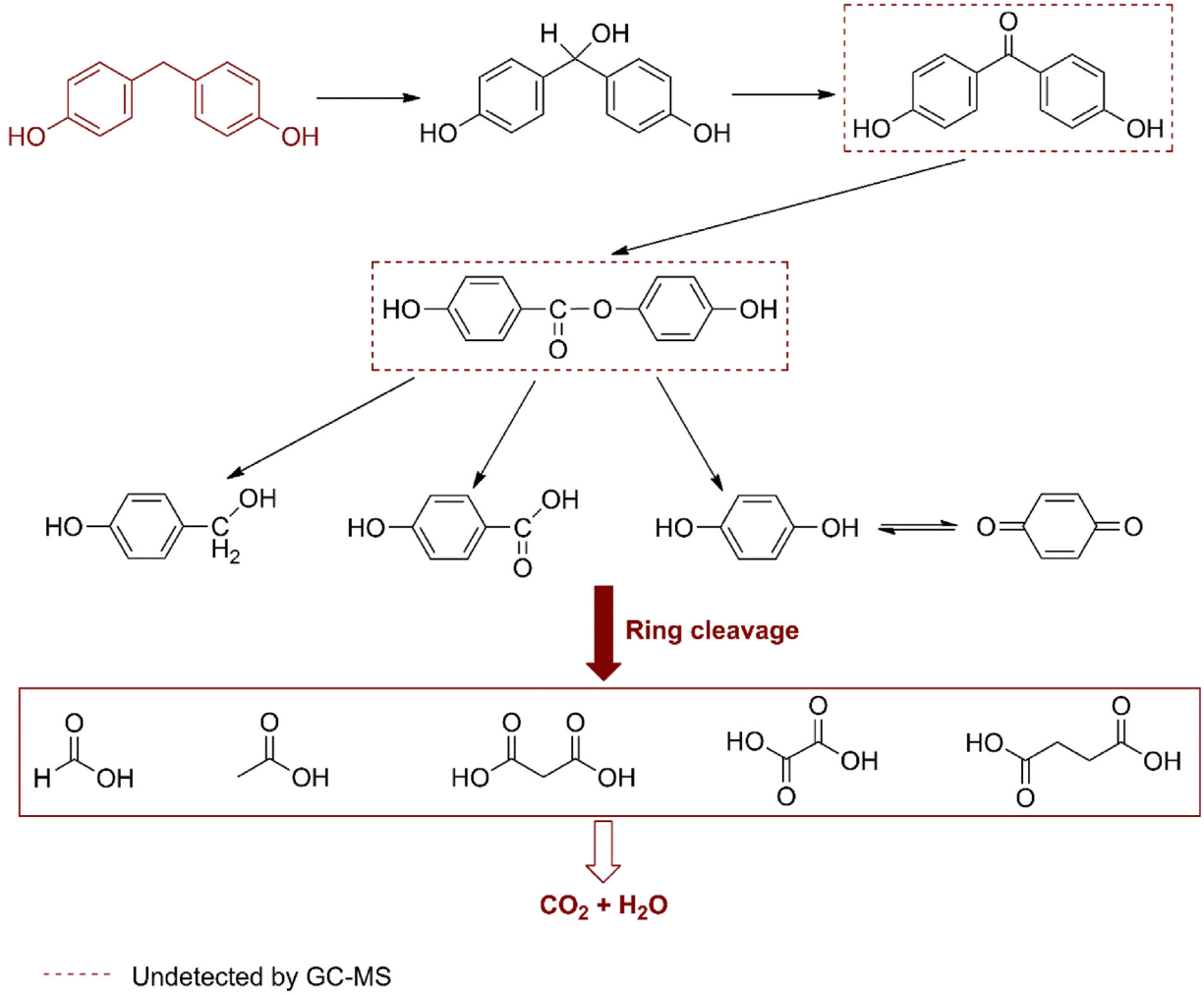

Fig. 17. Proposed pathway of BPF mineralization by the heterogeneous CeO_2-$LaCuO_3$/H_2O_2 process.

ual organic compounds adsorbed over the catalyst had a negative effect on its reusability in subsequent reactions [69]. CeO_2-$LaCuO_3$ appears, then, to be a promising catalyst for the oxidation of contaminated wastewaters by Fentonís process.

In addition, possible leaching of the reactive cupric and cerium ions in the reaction medium was checked. The leached amount of both metals after each runwas below the ICP detection limit (<0.01 mg L^{-1}). CeO_2-$LaCuO_3$ appears, then, to be a promising highly stable catalyst for the oxidation of contaminated wastewaters by Fentonís process.

10. Reaction pathway

HPLC analysis indicated that the gradual disappearance of the parent molecule (Bisphenol F) was accompanied by the formation of intermediate compounds. These intermediates were identified by GC–MS in order to elucidate a plausible reaction pathway for BF mineralization by the heterogeneous Fenton system. The corresponding experiment was performed at high concentration (200 mg L^{-1}) in order to ensure adequate detection. The initial solution and samples from different treatment times at pH 7.0 were analyzed. The identification was based on mass fragmentation values and by comparing the mass spectra to a database. Table 4 exhibits the mass spectra data of the 6 major products, including the molecular structures and characteristic fragment ions. Intermediates 1–6 were identified as 4-Hydroxybenzenemethanol, 4-Hydroxybenzaldehyde,Bis (4-hydroxyphenyl) methanol, 4-Hydroxybenzenemethanol, *p*-Benzoquinone and Hydroquinone, respectively. Fig. 15 shows the GC/MS profiles of BPF derivatives at different treatment times. As observed, the final analysis of samples after 5 h of treatment indicated the total elimination of all these compounds.

The possible reaction pathway of BPF mineralization involves primary the addition of hydroxyl radical on the aromatic ring of bisphenol F to give the hydroxylated derivativeBis (4-hyroxyphenyl) methanol, which is the primary produced intermediates. Further oxidation leads to the cleavage of the two benzene rings and the production of 4-hydroxybenzaldehyde, 4-Hydroxybenzenemethanol, *p*-benzoquinone and hydroquinone. From the benzene derived products formation, the authors speculated the formation of 4,4′ dihydroxybenzophenone and 4-hydroxyphenyl 4-hydroxybenzoate. Ultimate ring-opening of the cyclic intermediates leads to the formation of short chain organic acids of low molecule weight, which are generally reported as the end-products before mineralization to carbon dioxide and water [77,78]. Eventually, aliphatic acids, including malonic (tr = 20.66 min), succinic(tr = 21.83 min), oxalic(tr = 23.29 min), formic(tr = 6.21 min) and acetic (tr = 5.70 min)acids appear in the solution and were identified by anionic chromatography during the bisphenol F mineralization. The concentration of the above acids was determined via standard compounds and their evolution during the treatment is depicted in Fig. 16. Succinic and malonic acid

Table 4
GC–MS identification of the chemical structure, retention time and main mass fragmentation values of identified BPF intermediates formed during the heterogeneous Fenton process.

Identification number	compound	Main mass fragmentation value (m/z)	R_T(min)	Structure
I	p-Benzoquinone	108/82.1	6.932	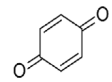
II	Hydroquinone	101.1/81	17.123	
III	4-Hydroxybenzenemethanol	124.1/106.0/95.1/77.1/65.1	19.154	
V	4-Hydroxybenzaldehyde4-hydroxybenzoate	121.0/107.0/93.1/75.0/65.1	19.566	
VI	Bis (4-hyroxyphenyl) methanol	200.1/183.0/107.1	35.431	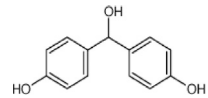

were the primary intermediates from the ring cleavage, oxalic and acetic acids were the ultimate and more persistent compounds. The high persistence of oxalic and acetic acids could explain the incomplete mineralization of BPF solutions reported in the above discussions.

Based on the identified intermediates products, the possible mineralization pathway for Bisphenol F is proposed in Fig. 17. The suggested mechanism is in agreement with that proposed by Inoue et al. [15] for the biodegradation of Bisphenol F, in which several of the identified intermediates coincided with the ones we found.

11. Conclusions

Ceria doped perovskites showed comparatively higher catalytic activity in terms of Bisphenol F and TOC removal than pristine perovskites. At pH 3, TOC removal followed the order of CeO_2-$LaCuO_3$ > CeO_2-$LaFeO_3$ > $LaCuO_3$ > $LaFeO_3$ > CeO_2. Ceria-perovskite composites exhibited good performance in terms of both catalytic activity and stability. The improvement in the catalytic activity of the nanoperovskites was ascribed to the enlargement of the surface area and, most importantly, to the synergistic effect between the transition element (iron or copper) and cerium. The ESR spectra and scavenger tests results indicate that the hydroxyl radicals ($^{\bullet}OH$) were the dominant reactive oxygen species generated during the catalytic treatment of bisphenol F under the heterogeneous Fenton system. The intermediates identification allowed proposing a degradation pathway for the mineralization of Bisphenol F with $^{\bullet}OH$. This study shows that the ceria-perovskite nanomaterials could potentially serve as excellent heterogeneous catalyst for organic compounds treatment. Moreover, the synergistic effects of cerium ions were pointed out, stimulating further investigation on the use of different transition metals as co-catalysts for enhancing the performance of heterogeneous Fenton/Perovskite process.

References

[1] R.F. Lane, C.D. Adams, S.J. Randtke, R.E. Carter Jr., Water Res. 79 (2015) 68–78.
[2] Y. Yang, L. Lu, J. Zhang, Y. Yang, Y. Wu, B. Shao, J. Chromatogr. A 1328 (2014) 26–34.
[3] S. Eladak, T. Grisin, D. Moison, M.J. Guerquin, T. N'Tumba-Byn, S. Pozzi-Gaudin, Fertil. Steril. 103 (2015) 11–21.
[4] B. Castro, P. Sánchez, J.M. Torres, E. Ortega, Environ. Res. 142 (2015) 281–287.
[5] C. Liao, K. Kannan, J. Agric. Food Chem. 61 (2013) 4655–4662.
[6] C. Liao, F. Liu, K. Kannan, Environ. Sci. Technol. 46 (2012) 6515–6522.
[7] J.R. Rochester, A.L. Bolden, Environ. Health Perspect. 123 (2015) 643–650.
[8] E. Danzl, K. Sei, S. Soda, M. Ike, M. Fujita, Int. J. Environ. Res. Public Health 6 (2009) 1472–1484.
[9] N. Cabaton, C. Dumont, I. Severin, Toxicology 255 (2009) 15–24.
[10] M. Audebert, L. Dolo, E. Perdu, J. Cravedi, D. Zalko, Arch. Toxicol. 85 (2011) 1463–1473.
[11] M.Y. Chen, M. Ike, M. Fujita, Environ. Toxicol. 17 (2002) 80–86.
[12] S. Kitamura, T. Suzuki, S. Seigo, R. Kohta, N. Jinno, K. Sugihara, S. Yoshihara, N. Fujimoto, H. Watanabe, H. Ohta, Toxicol. Sci. 84 (2005) 249–259.
[13] N. Cabaton, M.C. Chagnon, J.C. Lhuguenot, J.P. Cravedi, D. Zalko, J. Agric. Food Chem. 54 (26) (2006) 10307–10314.
[14] F. Pana, T. Xu, L. Yang, X. Jiang, L. Zhang, Acta Part A: Mol. Biomol. Spectrosc. 132 (2014) 795–802.
[15] D. Inoue, S. Hara, Mari Kashihara, Yusaku Murai, Erica Danzl, Kazunari Sei, Shinji Tsunoi, Masanori Fujita, M. Ike, Appl. Environ. Microbiol. 74 (2008) 352–358.
[16] M. Ike, M.-Y. Chen, E. Danzl, K. Sei, M. Fujita, Water Sci. Technol. 53 (2006) 153–159.
[17] H. Lu, Z. Weng, H. Wei, J. Zhou, J. Wang, G. Liua, W. Guo, J. Chem. Technol. Biotechnol. 92 (2017) 854–860.
[18] P. Katapodis, M. Moukouli, P. Christakopoulos, Int. Biodeter. Biodegr. 60 (2007) 267–272.
[19] Y. Chen, X.G. Xie, C.G. Ren, C.C. Dai, Bioresour. Technol. 129 (2013) 568–574.
[20] S. Esplugas, J. Giménez, S. Contreras, E. Pascual, M. Rodrıguez, Water Res. 36 (2002) 1034–1042.
[21] M. Antonopoulou, E. Evgenidou, D. Lambropoulou, I. Konstantinou, Water Res. 53 (2014) 215–234.
[22] M. Jovic, D. Manojlovic, D. Stankovic, B. Dojcinovi, B. Obradovic, U. Gasi, G. Roglic, J. Hazard. Mater. 260 (2013) 1092–1099.
[23] J.H. Ramirez, M.A. Vicente, L.M. Madeira, Appl. Catal. B Environ. 98 (2010) 10–26.
[24] S. Ben Hammouda, N. Adhoum, L. Monser, J. Hazard. Mater. 301 (2016) 350–361.
[25] S. Ben Hammouda, N. Adhoum, L. Monser, J. Hazard. Mater. 294 (2015) 128–136.
[26] F. Martínez, M.I. Pariente, J. Ángel, J.A. Botas, J.A. Melero, A. Rubalcaba, J. Chem. Technol. Biotechnol. 87 (2012) 880–886.
[27] A. Santos, P. Yustos, S. Rodríguez, F. Garcia-Ochoa, M. Gracia, Ind. Eng. Chem. Res. 46 (2007) 2423–2427.
[28] M. Aleksić, H. Kušić, N. Koprivanac, D. Leszczynska, A.L. Božić, Desalination 257 (2010) 22–29.
[29] R. Gonzalez-Olmos, M.J. Martin, A. Georgi, F.D. Kopinke, I. Oller, S. Malato, Appl. Catal. B Environ. 125 (2012).
[30] A.N. Soon, B.H. Hameed, Appl. Catal. A-Gen. 450 (2013) 96–105.
[31] S. Parra, L. Henao, E. Mielczarski, J. Mielczarski, P. Albers, E. Suvorova, Langmuir 20 (2004) 5621–5629.
[32] R.M. Liou, S.H. Chen, M.Y. Hung, C.S. Hsu, J.Y. Lai, Chemosphere 59 (2005) 117–125.
[33] R.M. Liou, S.-H. Chen, M.-Y. Hung, C.-S. Hsu, Chemosphere 55 (2004) 1271–1280.
[34] L.F. Liottaa, M. Gruttadauria, G. Di Carlo, G. Perrini, V. Librando, J. Hazard. Mater. 162 (2009) 588–606.
[35] L. Chirchi, A. Ghorbel, Appl. Clay Sci. 21 (2002) 271–276.
[36] Y. Sun, S.S. Hla, G.J. Duffy, A.J. Cousins, D. French, L.D. Morpeth, J.H. Edwards, D.G. Roberts, Int. J. Hydrogen Energy 36 (2011) 79–86.
[37] P. Shikha, T.S. Kang, B.S. Randhawa, J. Alloy Compd. 625 (2015) 336–345.

[38] V.N. Stathopoulos, V.C. Belessi, T.V. Bakas, S.G. Neophytides, C.N. Costa, P.J. Pomonis, A.M. Efstathiou, Appl. Catal. B 93 (2009) 1–11.
[39] H. Tanaka, M. Misono, Curr. Opin. Solid State Mater. Sci. 5 (2001) 381–387.
[40] Z. Zhong, K. Chen, Y. Ji, Q. Yan, Appl. Catal. A: Gen. 156 (1997) 29–41.
[41] L.G. Tejuca, J.L.G. Fierro, J.M.D. Tascón, Adv. Catal. 36 (1989) 237–328.
[42] T. Nitadori, M. Misono, J. Catal. 93 (1985) 459–466.
[43] M. Alifanti, M. Florea, V. Cortes-Corberan, U. Endruschat, B. Delmon, V.I. Pârvulescu, Catal. Today 112 (2006) 169–173.
[44] A.K. Ladavos, P.J. Pomonis, Appl. Catal. B: Environ. 2 (1993) 27–47.
[45] S. Colonna, D. de Rossi, M. Faticanti, I. Pettiti, P. Porta, J. Mol. Catal. A: Chem. 187 (2002) 269–276.
[46] S. Cimino, S. Colonna, S. de Rossi, M. Faticanti, L. Lisi, I. Pettiti, P. Porta, J. Catal. 205 (2002) 309–317.
[47] X.P. Xiang, L.H. Zhao, B.T. Teng, J.J. Lang, X. Hu, T. Li, Y.A. Fang, M.F. Luo, J.J. Lin, Appl. Surf. Sci. 276 (2013) 328–332.
[48] T.H. Shin, S. Ida, T. Ishihara, Doped CeO2 −LaFeO3 composite oxide as an active anode for direct hydrocarbon-type solid oxide fuel cells, J. Am. Chem. Soc. 133 (2011) 19399–19407.
[49] L. Liu, K. Sun, X. Li, M. Zhang, Y. Liu, N. Zhang, X. Zhou, Int. J. Hydrogen Energy 37 (2012) 12574–12579.
[50] I. Miguel-García, S. Parres-Esclapez, D. Lozano-Castelló, A. Bueno-López, Catal. Commun. 11 (2010) 848–852.
[51] Y. Wang, J. Zhu, L. Zhang, X. Yang, L. Lu, X. Wang, Mater. Lett. 60 (2006) 1767–1770.
[52] F. Touahra, A. Rabahi, R. Chebout, A. Boudjemaa, D. Lerari, M. Sehailia, D. Halliche, K. Bachari, Int. J. Hydrogen Energy 41 (2016) 2477–2486.
[53] C.G. Maciel, T.F. Silva, M.L. Hirooka, M.N. Belgacem, J.M. Assaf, Fuel 97 (2012) 245–252.
[54] M.N. Guo, C.X. Guo, L.Y. Jin, Y.J. Wang, J.Q. Lu, M.F. Luo, Mater. Lett. 64 (2010) 1638–1640.
[55] L. Bocher, M.H. Aguirre, R. Robert, M. Trottmann, D. Logvinovich, P. Hug, A. Weidenkaff, Thermochim. Acta 457 (2007) 11–19.
[56] R. Hu, R. Ding, J. Chen, J. Hu, Y. Zhang, Catal. Commun. 21 (2012) 38–41.
[57] NIST X-ray photoelectron spectroscopy database. Measurement Services Division of the National Institute of Standards and Technology (NIST) Technology Services, 2008.
[58] K. Wang, H. Niu, J. Chen, J. Song, C. Mao, S. Zhang, S. Zheng, B. Liu, C. Chen, Materials 9 (2016) 326–338.
[59] O.P. Taran, A.B. Ayusheev, O.L. Ogorodnikova, I.P. Prosvirin, L.A. Isupova, V.N. Parmon, Appl. Catal. B 180 (2016) 86–93.
[60] L. Xu, J. Wang, Environ. Sci. Technol. 46 (2012) 10145–10153.
[61] D.E. Shahwar, A. Yasar, S. Yousaf, Solar assisted photo Fenton for cost effective degradation of textile effluents in comparison to AOPs, Global Nest J. 14 (2012) 477–486.
[62] Y. Liu, J. Xie, C. Nam Ong, C.D. Vecitisc, Z. Zhou, Environ. Sci.: Water Res. Technol. 1 (2015) 769–778.
[63] L. Xu, J. Wang, Environ. Eng. Sci. 30 (2013) 294–301.
[64] R. Karale, B. Manu, S. Shrihari, Int. J. Adv. Technol. Civil Eng. 2 (2013) 34–38.
[65] E. Neyens, J. Baeyens, J. Hazard. Mater. 98 (2003) 33–50.
[66] L. Xu, J. Wang, Environ. Sci. Technol. 46 (2012) 10145–10153.
[67] A. Dhaouadi, L. Monser, N. Adhoum, Electrochim. Acta 54 (2009) 4473–4480.
[68] J.L. Sotelo, G. Ovejero, F. Martínez, J.A. Melero, A. Milieni, Appl. Catal. B. 47 (2004) 281–294.
[69] L. Zhang, D. Xu, C. Hu, Y. Shi, Appl. Catal. B 207 (2017) 9–16.
[70] J.M. Fontmorin, R.C.B. Castillo, W.Z. Tang, M. Sillanpää, Water Res. 99 (2016) 24–32.
[71] A. Goi, Y. Veressinina, M. Trapido, Chem. Eng. J. 143 (2016) 1–9.
[72] A.D. Bokare, W. Choi, J. Hazard. Mater. 275 (2014) 121–135.
[73] G. Zhang, J. Long, X. Wang, Z. Zhang, W. Dai, P. Liu, Z. Li, L. Wu, X. Fu, Langmuir 26 (2010) 1362–1371.
[74] S.H. Joo, A.J. Feitz, D.L. Sedlak, T.D. Waite, Environ. Sci. Technol. 39 (2005) 1263–1268.
[75] K. Ayoub, S. Nélieu, E.D. van Hullebusch, Alessandra Maia-Grondard, Michel Cassir, A. Bermond, Chem. Eng. J. 173 (2011) 309–317.
[76] G.V. Buxton, C.L. Greenstock, W.P. Helman, A.B. Ross, J. Phys. Chem. Ref. Data 7 (1988) 513–886.
[77] M.A. Oturan, M. Pimentel, N. Oturan, I. Sirés, Electrochim. Acta 54 (2008) 173–182.
[78] S. Garcia-Segura, E. Brillas, Water Res. 45 (2011) 2975–2984.